Photophysics of *trans*-4-(Dimethylamino)-4′-cyanostilbene and Its Use as a Solvation Probe

Sergei Arzhantsev,[†] Klaas A. Zachariasse,[‡] and Mark Maroncelli*[,†]

Department of Chemistry, The Pennsylvania State University, University Park, Pennsylvania 16802, and Max-Planck-Institut für Biophysikalische Chemie, Spektroskopie und Photochemische Kinetik, 37070 Göttingen, Germany

Received: October 16, 2005; In Final Form: January 9, 2006

Electronic structure calculations, steady-state electronic spectroscopy, and femtosecond time-resolved emission spectroscopy are used to examine the photophysics of *trans*-4-(dimethylamino)-4′-cyanostilbene (DCS) and its solvent dependence. Semiempirical AM1/CI calculations suggest that an anilino TICT state is a potential candidate for the emissive state of DCS in polar solvents. But observation of large and solvent-independent absorption and emission transition moments in a number of solvents ($M_{abs} = 6.7 \pm 0.4$ D and $M_{em} = 7.6 \pm 0.8$ D) rule out the involvement of any such state, which would have a vanishingly small transition moment. The absorption and steady-state emission spectra of DCS evolve in a systematic manner with solvent polarity, approximately as would be expected for a single, highly polar excited state. Attempts to fit the solvatochromism of DCS using standard dielectric continuum models are only partially successful when values of the solute dipole moments suggested by independent measurements are assumed. The shapes of the absorption and emission spectra of DCS change systematically with solvent polarity in a manner that is semiquantitatively reproduced using a coupled-state model of the spectroscopy. Kerr-gate emission measurements show that the emission dynamics of DCS down to subpicosecond times reflect only solvent relaxation, rather than any more complicated electronic state kinetics. The spectral response functions measured with DCS are well correlated to those previously reported for the solvation probe coumarin 153, indicating DCS to be a useful alternative probe of solvation dynamics.

I. Introduction

DCS, *trans*-4-(dimethylamino)-4′-cyanostilbene (Scheme 1), is one member of a family of "push−pull" stilbenes,[1,2] which have long attracted attention for the charge-transfer character of their excited states[3] and for the large optical nonlinearities this character provides.[4,5] Studies of DCS itself extend as far back as the 1950s when Lippert first estimated the excited-state dipole moment of DCS from solvatochromic measurements.[6] Lippert's work and many subsequent studies clearly established the charge-transfer character of the $S_0 \leftrightarrow S_1$ transition of DCS.[7−11] Other studies[12] showed that the primary deactivation pathway of S_1 DCS is related to the trans−cis isomerization common to most stilbene derivatives.[1] Detailed studies of the solvent dependence of the trans−cis isomerization rates and spectroscopy of DCS were carried out by Zachariasse and co-workers.[10,13] They showed that the highly polar nature of the trans-emitting state renders isomerization to the nonemissive cis state strongly dependent on the polarity of the solvent. For example, in the nearly isoviscous solvents acetonitrile and heptane, the fluorescence lifetimes (approximate isomerization times) are 546 and 72 ps, respectively.[13] Semiempirical[4,14,15] and ab initio[16−19] calculations as well as supersonic jet spectroscopy[20,21] have also been used to help understand the structure and electronic states relevant to this photochemistry. Finally, quite a few time-resolved studies have focused on the early-time spectral dynamics, that is, the dynamics prior to isomerization, of *trans*-DCS in polar solvents.[9,10,13,22−29] These latter studies have generated a variety of conflicting views of the nature of the state or states that give rise to the fluorescence of *trans*-DCS in polar solvents.

SCHEME 1

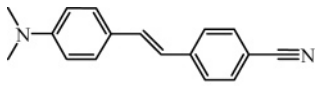

DCS = *trans*-4-dimethylamino-4'-cyanostilbene

In the first study of the early emission dynamics of DCS, Safarzadeh-Amiri used the time-correlated single photon counting (TCSPC) method with ∼200 ps time resolution[22] to observe the emission of DCS in low-temperature butanol and glycerol. Citing the results of the seminal study on DCS photophysics by Gruen and Görner,[12] Safarzadeh-Amiri interpreted the observed emission kinetics in terms of solvation of a single excited state and showed that the spectral evolution takes place over times that agree with the predictions of dielectric continuum models of solvation. Two years later, Rulliere and co-workers used Kerr-gated emission spectroscopy (∼80 ps resolution) to measure time-resolved spectra of DCS in several solvents.[23] In all of the polar solvents studied, they observed dual emission which they interpreted in terms of two distinct emitting states. Analogy with 4-dimethylaminobenzonitrile, as well as other arguments,[30] led these authors to attribute the dual emission to the formation of an emissive twisted intramolecular charge-transfer (TICT) state from the state initially reached upon electronic absorption. Later work by Rulliere and co-workers[9,24−27] showed that dual emission is only observed in concentrated

* To whom correspondence should be addressed. E-mail: Maroncelli@psu.edu.
[†] The Pennsylvania State University.
[‡] Max-Planck-Institut für Biophysikalische Chemie, Spektroskopie und Photochemische Kinetik.

10.1021/jp0559231 CCC: $33.50
Published on Web 02/23/2006

solutions and under conditions of high excitation intensity. They proposed that under these conditions a "bicimer" is formed between two excited-state molecules. In the absence of these bimolecular processes, the emission of DCS, at least at times >80 ps, was reported to entail only a dynamic Stokes shift[9] as initially found by Safarzadeh-Amiri.[22] Nevertheless, differences between various constrained analogues of DCS led Rulliere and co-workers to propose a rather complicated description of the excited-state evolution of DCS, involving <1 ps relaxation from the Franck−Condon state to a polar intramolecular charge-transfer (ICT) state and then subsequent relaxation to a "conformationally relaxed" ICT state.[27]

In support of the existence of more than one emitting state, Eilers-Koenig et al.[31] reported that subpicosecond fluorescence upconversion data of DCS in acetonitrile appear to show the presence of an isoemissive point at early times. Comparable data in methanol did not show such a stationary point.[31] The steady-state solvatochromism of DCS was also interpreted by Il'ichev et al.[10] to imply a transition between the Franck−Condon state to a state of higher polarity prior to emission. But these authors did not observe evidence for a transition in their time-resolved experiments and concluded that the FC → ICT transition must occur before 5 ps, probably in the subpicosecond time domain.[10] More recently, Pines et al.[29] reported time-resolved emission spectra (20 ps resolution TCSPC experiments) of two DCS analogues in ethanol which also show apparent isoemissive points. These authors analyzed their data in terms of a transition between a locally excited state and a charge-transfer state reached by twisting about the aniline group, occurring on a time scale of 4−8 ps. This suggestion of the involvement of anilino TICT states was supported by the recent electronic structure calculations of Amatatsu[16,17] as well as earlier work.[14]

In contrast, the most recent experiments by Ernsting and co-workers[28] refute the idea that there is anything more than a single electronic state responsible for the emission of DCS. These workers performed broad-band fluorescence upconversion and transient absorption measurements on DCS in acetonitrile with sub-100 fs time resolution.[28] They studied the concentration and intensity dependence of the spontaneous emission and transient absorption spectra and provided convincing evidence that the dual emission observed by Rulliere and co-workers[9,23−27] is not due to bicimer formation but is rather the result of the reabsorption of fluorescence by excited molecules. Contrary to the results of Eilers-Koenig et al.,[31] in the absence of reabsorption, their fluorescence spectra of DCS in acetonitrile display only a continuous spectral shift over times characteristic of solvent relaxation. Ernsting and co-workers showed that the time dependence of this shift matches remarkably well with the predictions of a dielectric continuum description of solvation, leading them to conclude that "solvation is the only relaxation process on the ps time scale"[28] in DCS. Whether the same conclusion applies to solvents other than acetonitrile was not established.

The foregoing review reveals a broad spectrum of views concerning the emission dynamics of DCS. Interpretations range from the dynamics being only that of a time-evolving Stokes shift resulting from solvent equilibration in a single electronic state[28] all the way to models invoking transitions among 2−3 distinct emitting states.[26,27] Intermediate cases of continuous evolution on a nearly barrierless surface of variable charge-transfer character are also possible.[10]

In the present work, we seek to clarify this situation through additional data and a new analysis of the solvent dependence of the steady-state electronic spectra of DCS and through subpicosecond time-resolved emission measurements. We also examine the predictions of electronic structure calculations in order to add perspective to our experimental observations and past computational work. Although there remain some unresolved difficulties in completely modeling its solvatochromism, we find no evidence that more than a single electronic state contributes to the emission of DCS. The near constancy of the absorption and emission transition moments observed here argues strongly against any large change in the makeup of S_1, either between absorption and emission or as a function of solvent. The predictions of electronic structure calculations make it especially clear that emission from a state of significant TICT character cannot be consistent with the observed transition moments. In a range of solvents, emission spectra even on a 100 fs time scale appear to reflect only the dynamics of polar solvation as Kovalenko et al.[28] found in the case of acetonitrile. Comparisons to prior results on the solute coumarin 153 indicate that DCS reports on polar solvation dynamics in much the same way as does this well-established solvation probe. We therefore propose DCS as an alternative probe of solvation and solvation dynamics, which, because of its shorter lifetime and larger Stokes shift, offers advantages for use in some applications such as Kerr-gated emission spectroscopy.

II. Experimental Methods

trans-4-Dimethylamino-4′-cyanostilbene (DCS) was synthesized and purified according to the procedure described in ref 10. NMR measurements indicated <5% contamination from *cis*-DCS in the crystalline sample. Solvents used in this work were of HPLC or spectrophotometric grade (typically >99%) from Sigma-Aldrich and were used as received, except for possible drying over molecular sieves.

Steady-state absorption and emission measurements were made using a Hitachi U-3010 UV−vis spectrophotometer and a PTI QuantaMaster 1 spectrometer, respectively. Samples for emission spectroscopy were prepared in 1 cm quartz cuvettes to have optical densities at the S_1 absorption maximum of less than 0.1. These samples were not deoxygenated. Absorption frequencies were typically measured using such dilute samples, but more concentrated samples were prepared (OD ∼ 1) at the S_1 maximum for determining extinction coefficients and absorption transition moments. Emission quantum yields were measured relative to quinine sulfate dehydrate in 0.05 M H_2SO_4 ($\phi_{em} = 0.508$[32]) according to

$$\varphi_S = \varphi_R \left(\frac{{n_R}^2}{{n_S}^2}\right)\left(\frac{I_S}{I_R}\right)\left(\frac{1 - 10^{-0.5A_R}}{1 - 10^{-0.5A_S}}\right) \quad (1)$$

All steady-state measurements were performed at 25 ± 0.1 °C.

Time-resolved emission measurements were made using two instruments. The fluorescence lifetimes needed for radiative rate determinations employed a 25 ps time-correlated single photon counting apparatus (see ref 33 for details). Subpicosecond time-resolved emission spectra were recorded with a Kerr-gated emission spectrometer. This instrument and its use are described in detail in ref 34. Briefly, the doubled output of a 250 kHz amplified Ti:sapphire laser (775 nm, 160 fs, 3 μJ) is used for the excitation of a sample contained in a 1 mm quartz flow cell. Samples were made up to have optical densities of approximately 0.2. Spontaneous emission from the sample is routed through a Kerr shutter comprised of a 1 mm liquid benzene cell placed between crossed polarizers. A delayed pulse of the laser fundamental is used to gate the emission, which is

SCHEME 2

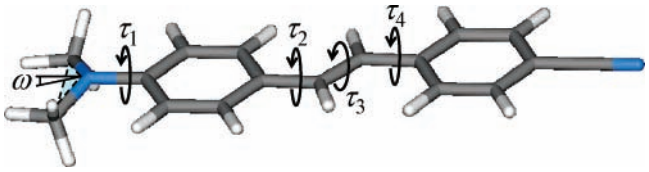

dispersed by a monochomator + CCD combination used to record the instantaneous spectrum over the range 400−650 nm. Spectra are later corrected for the wavelength-dependent temporal dispersion of the collection optics and the wavelength-dependent sensitivity of the detectors. The instrument response of the system, as judged by the signal from solvent Raman bands, is 450 fs (full width at half maximum, fwhm). Deconvolution of the data affords resolutions of better than 100 fs, comparable to those achieved with fluorescence upconversion. All of the Kerr-gated emission experiments reported here were performed at room temperature, 20 ± 1 °C.

trans-DCS readily isomerizes in solution when exposed to UV light. We made some attempts to characterize this process to ensure that it did not interfere with our measurements. Exposure to room light for short periods of time has relatively little effect on the spectrum *trans*-DCS, however, exposure of more than a few hours leads to noticeable changes to the absorption spectrum and significant reduction in emission yield due to the buildup of the cis photoproduct. Whereas we found that little care was needed to record an absorption spectrum without causing significant degradation, use of the excitation light intensities we normally employ for steady-state and time-resolved emission spectroscopy produced significant loss of emission intensity during the time required to record data. No change in the shape of the emission spectrum or in the characteristics of the time-resolved emission (femtosecond−nanosecond time scales) could be detected, however. These observations hold even in samples reaching a photostationary state, which is expected to consist of comparable amounts of cis and trans isomers.[1] Thus, at least on time scales of >100 fs, the cis isomer appears to be completely nonfluorescent, and its presence does not interfere with most of the measurements made here. For convenience, the samples used for the femtosecond time-resolved measurements therefore consisted of mixtures of cis and trans isomers under approximately photostationary conditions. In contrast, for measurements of accurate absorption spectra and especially for emission quantum yield determinations, care was taken to avoid any unnecessary exposure to light. Samples for such measurements were prepared under red light and stored in the dark prior to use. Such samples remain unchanged for periods of many weeks. When recording spectra of these samples, excitation energies were maintained at such a sufficiently low level that isomerization was minimized (<30% emission intensity decrease per hour, compared to the 4 min needed to record a spectrum). With these precautions, we believe that all of the results presented here are representative of the photophysics of pure *trans*-DCS.

III. Electronic Structure Calculations

To help characterize the electronic properties of DCS, we performed ab initio and DFT calculations using the Gaussian03[35] program and semiempirical calculations with AMPAC 8.[36] Optimization of the ground state of *trans*-DCS using the AM1 and RHF/6-31G(d,p) methods produces significantly nonplanar structures of the stilbene portion of the molecule. Denoting torsional angles according to Scheme 2, these methods predict that the phenyl groups are twisted by approximately 20° relative to the central double bond (τ_2 and τ_4, Table 1). B3LYP/6-31G-(d,p) calculations, on the other hand, predict an essentially planar stilbene framework, as did the prior calculations of Amatatsu.[16] Such variability is consistent with recent calculations on the parent molecule stilbene, which show that these torsional potentials are sensitive to details of the basis set and correlation level employed.[37] We note that both the AM1 and RHF/6-31G-(d,p) calculations predict that the planar structure lies less than 2 kJ/mol higher in energy than the optimally twisted forms. Furthermore, the RHF and B3LYP calculations show that concerted twisting about τ_2 and τ_4 occurs at very low frequencies, 23 and 9 cm^{-1}, respectively. At room temperature, molecules will therefore be distributed over a broad range of angles centered on the planar structure,[4,38] whether or not it is a true minimum as in the case of stilbene itself.[37,39] Because the calculated properties are not very sensitive to the twist angle over the relevant range, in the remaining discussion, we assume a planar stilbene framework for the trans molecule.

The dipole moment of *trans*-DCS in the ground state is calculated to be between 6 and 10 D, with the calculations expected to be the most accurate when predicting values close to 8 D (Table 1). The experimental value, measured in benzene and dioxane solution, is somewhat smaller, 7.0 D.[40] Figure 1 provides a representation of the ground-state charge distribution of DCS in terms of electrostatic potential fit charges. The dipole moment lies nearly parallel to the long inertial axis of the molecule and is produced by a charge distribution consisting of net charges of +0.11, −0.16, and +0.05 *e* on the dimethylanilino, ethylenic, and benzonitrile portions of the molecule.

Properties of the S_1 state of DCS were calculated using the AM1/CI method, and some results of these calculations are summarized in Table 2. The CI employed here entailed mixing of approximately 1200 energy-selected microstates from single and multiple excitations of electrons among the 10 states surrounding the highest occupied molecular orbital to lowest unoccupied molecular orbital (HOMO−LUMO) gap.[36] These calculations predict the geometry of the S_1 state to be planar with respect to both the stilbene framework and the dimethylamino group. The dipole moment of S_1 is calculated to be 14.5 D and oriented within 5° of the S_0 dipole direction. Electrochromic absorption and emission measurements indicate values of between 20 and 21 D for μ_1 in dioxane[3,40,41] and cyclohexane,[8] considerably higher than the calculated value. (Many estimates of the S_1 moments have also been made on the basis of solvatochromic measurements,[6−11] but these results are less definitive, as will be discussed in detail in section VI.) Although there will be some (∼15%) enhancement of the dipole moment in solution compared to the gas phase,[42] it appears that the AM1/CI calculations significantly underestimate the increased charge separation in the excited state. As shown in Table 2, the same is true of higher-level CASSCF calculations,[17] whereas lower-level CNDO calculations[14] predict values closer to experiment. The difference between the S_1 and S_0 charge distributions (both from AM1/CI calculations) and the difference dipole $\Delta\vec{\mu} = \vec{\mu}_1 - \vec{\mu}_0$ (8.3 D) are illustrated on the bottom panel of Figure 1. The charge redistribution predicted is such that a charge of +0.27 *e* shifts from the anilino ring to the ethylenic (−0.10 *e*) and benzonitrile (−0.17 *e*) portions of the molecule. As shown in Table 2, the transition energy and oscillator strength are reasonably reproduced by the AM1/CI method.

We have also performed a number of AM1/CI calculations of different excited-state geometries of DCS to help address the question of whether multiple excited states might be

TABLE 1: Calculated Properties of Isolated (S_0) DCS

	trans				cis	
method	τ_2/deg[a]	τ_4/deg[a]	ω/deg[a]	μ/D	μ/D[a]	$\Delta E(c-t)$/kJ mol^{-1} [a]
AM1	16	23	22	6.13	3.58	7.8
RHF/6-31G(d,p)	17	23	28	8.26	6.24	16
RHF/6-31G(d,p) − *t*-planar[b]	(0)	(0)	21	8.47		15
B3LYP/6-31G(d,p)	0	0	10	9.83	7.05	22
MP2/6-311G(d,p)//RHF/6-31G(d,p)	(17)	(23)	(28)	7.86	5.65	7.1
CASSCF/pDZ//RHF/pDZ[c]	0	0	33	7.71		

[a] τ_2, τ_4, and ω refer to the angles shown in Scheme 2. μ is the permanent dipole moment. $\Delta E(c-t)$ is the energy difference between the cis and trans conformations. [b] *t*-Planar refers to a partial optimization of *t*-DCS in which all of the stilbene ring atoms are constrained to be coplanar. [c] From refs 16 and 17.

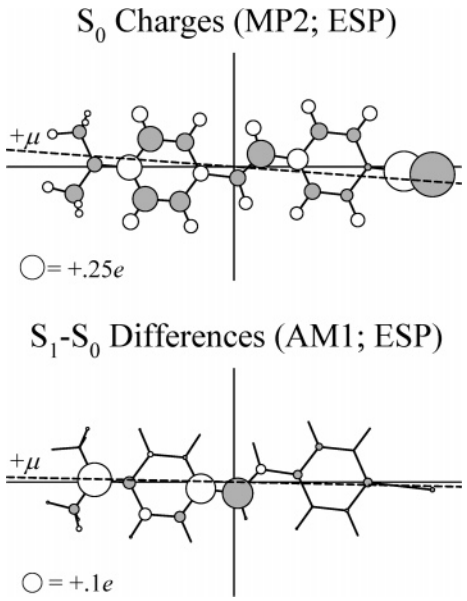

Figure 1. ESP-fit atomic charges of DCS in the ground state from MP2/6-311G(d,p) calculations (top) and $S_1 - S_0$ charge differences from AM1/CI calculations (bottom). Charge magnitudes are proportional to the radii of the circles as indicated. Open circles denote positive charge, and filled circles denote negative charge. The orientations of the ground-state dipole moment (top) and difference dipole $\vec{\mu}_1 - \vec{\mu}_0$ are indicated (dashed lines) relative to the inertial axes (solid).

TABLE 2: Calculated Properties of Isolated S_0 and S_1 *trans*-DCS[a]

method	μ_0/D	μ_1/D	ΔE[b]/eV	f	ref
AM1/CI	6.21	14.5	3.38	0.96	this work
CNDO/S	6.76	18.7	3.82	0.75	14
(8,9)CASSCF/pDZ	7.71	15.7	5.15 (3.69)[c]	1.26	17
expt	7.0[d]	21[d]	3.29	0.6−0.8[e]	

[a] All results are for a planar stilbene framework. μ_0 and μ_1 are the S_0 and S_1 dipole moments, ΔE the vertical energy gap, and f the oscillator strength of the $S_0 \rightarrow S_1$ transition. [b] Computed values are vertical excitation energies. The experimental value is from the absorption maximum in hexane. [c] Amatatsu[17] showed that the high value of 5.15 eV obtained using the CASSCF method could be brought into better agreement with that of the experimental by applying a multireference MP2 correction. [d] Reference 40. [e] These values represent the range observed in various solvents.

responsible for the emission of DCS in solution. More detailed and sophisticated calculations have already been performed by Amatatsu for this purpose,[16−18] who concluded that in polar solvents the emitting state is the twisted intramolecular charge-transfer (TICT) state that results from a 90° twist about the anilino bond[16,17] (τ_2 in Scheme 2). Lapoudyade et al.,[14] who performed CNDO/S calculations of variously twisted forms of DCS, also cited this geometry as a likely candidate for the emitting state in polar solvents. Figure 2 shows the AM1/CI

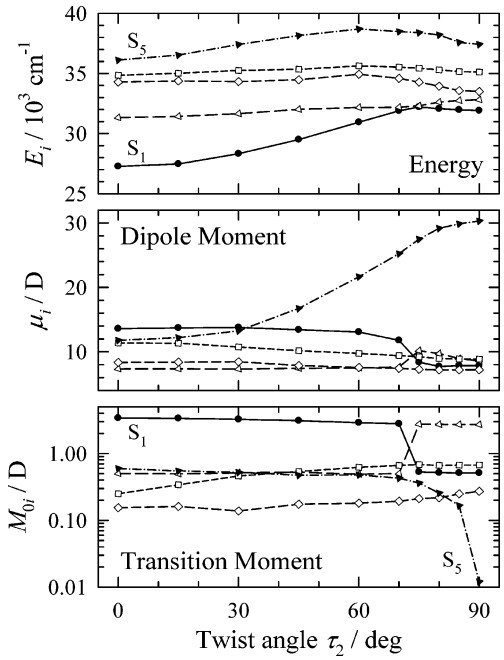

Figure 2. Gas-phase energies E, dipole moments μ, and transition dipole moments with the ground-state M_{0i}, of the lowest five singlet states S_1−S_5 of DCS as functions of the anilino twist angle (τ_2 in Scheme 2). These results are from AM1/CI calculations in which the geometry of the stilbene ring system has been constrained to be planar with the exception of the τ_2 angle and the remaining coordinates optimized. The two states of particular interest, S_1 and S_5, are shown with filled symbols. Note that the character of the $S_1(0°)$ state interchanges with that of the $S_2(0°)$ state near $\tau_2 = 73°$ as a result of an avoided crossing.

predictions for the lowest excited states as functions of the putative TICT coordinate τ_2. The states of interest are S_1 and S_5, shown with filled symbols. In the planar geometry, the S_1 state consists mainly of the HOMO → LUMO excitation (72% + 10% from HOMO → LUMO + 2). Figure 3 illustrates the nature of the molecular orbitals involved. In the planar geometry, the HOMO and LUMO orbitals are primarily located on the donor and acceptor portions of the molecule, but there is considerable delocalization of both orbitals over the whole π system. The $S_0 \rightarrow S_1$ transition thus entails only a fraction of a full electron transfer from the anilino fragment to the remainder of the molecule, which leads to a calculated S_1 dipole moment of ∼15 D. The TICT state (S_5, $\tau_2 = 90°$) is also dominated by the HOMO → LUMO excitation (98%), and the molecular orbitals are of similar character to those in the planar geometry. The main difference is that at 90° the anilino π orbitals are completely decoupled from the remaining π orbitals so that the HOMO → LUMO excitation entails a full electron transfer from the donor to the acceptor and thereby generates a huge dipole moment of 30 D. Other calculations provide similarly large

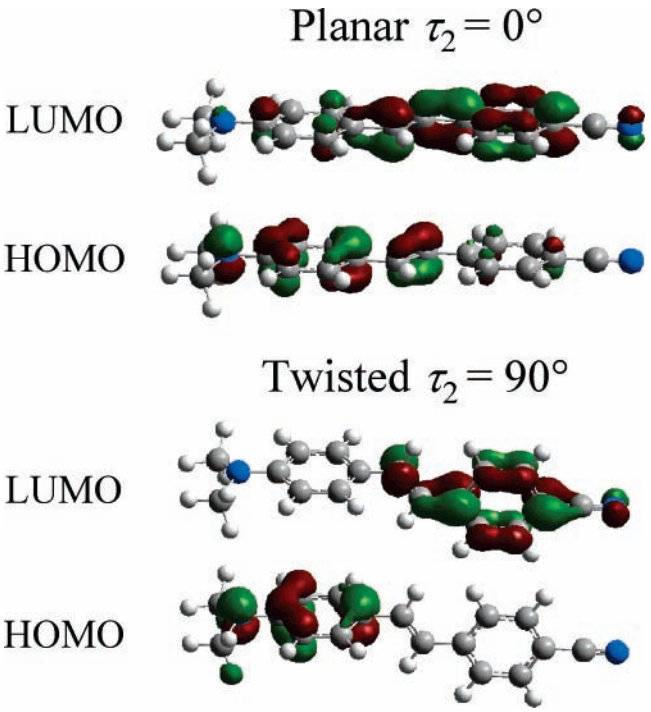

Figure 3. Frontier molecular orbitals calculated for the planar and twisted geometries of DCS.

dipole moments of the TICT state (29,[16] 35,[17] and 46 D[14]). In the gas phase, all calculations place the TICT state well above the planar S_1 state in energy. But the dipole moment of the TICT state is large enough relative to the dipole moments of the remaining states that dielectric continuum estimates locate the TICT state close to or lower in energy than the $S_1(0°)$ state in polar solvents.[16] Moreover, self-consistent reaction field calculations by Amatatsu have shown that there is little energy barrier to twisting in a polar solvent such as dimethyl sulfoxide.[17]

Such observations have led some workers to propose that the TICT state is probably responsible for DCS emission in polar solvents.[14,16,17] However, one prediction of the calculations illustrated in Figure 2 argues strongly against this interpretation. The same decoupling of the donor and acceptor π systems that leads to full charge separation also breaks the spectroscopic coupling between the TICT and ground states and leads to a precipitous drop in the transition moment M_{05}. Among all of the states predicted by these calculations, only the $S_1(0°)$ state is strongly coupled to the ground state, with a predicted transition moment of 3.4 D. The experimental values, discussed later, are in the range of 6−8 D. States S_2-S_4 possess much smaller transition moments, which do not change dramatically (apart from the $S_1 \leftrightarrow S_2$ identity reversal) with twist angle. S_5, in contrast, begins as a weak transition near $\tau_2 = 0$ and becomes essentially forbidden at $\tau_2 = 90°$. If this state played a significant and solvent-polarity-dependent role in the emission of DCS, then one would expect very large changes in the emission strength with the solvent. As described in section V, such changes are definitely not observed. Thus, the calculations appear to be incorrect in the prediction that an anilino TICT state is energetically favored in polar solvents.

Finally, we briefly mention what electronic structure calculations predict for the cis isomer of DCS. Some results are provided in Table 1. All of the methods examined here predict the ground state of the trans isomer to be the lower energy form in the gas phase by at least 7 kJ/mol. RHF and B3LYP predictions for the harmonic free energies at 298 K favor the trans isomer by 18 and 29 kJ/mol. All methods also predict the

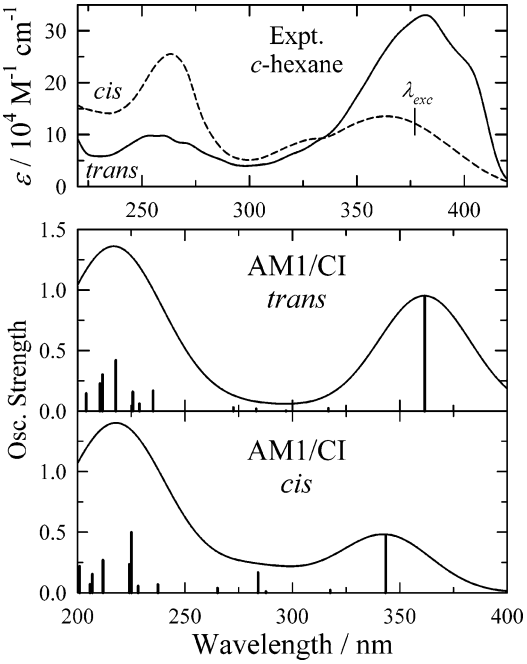

Figure 4. Absorption spectra of trans and cis isomers of DCS. The top panel shows experimental spectra in cyclohexane solvent obtained from an analysis of a series of spectra as a function of irradiation time beginning with a pure *trans*-DCS sample. (These spectra are comparable to spectra of cis and trans isomers separated by HPLC.[83]) The vertical scale of the experimental cis spectrum is only approximate. It was set by assuming a ratio of cis/trans maximum extinction coefficients of 0.41 for the 350 nm band, based on the spectra of stilbene and *trans*-4-(dimethylamino)-4′-nitrostilbene.[1] The lower panels show AM1/CI calculated spectra in the gas phase. The stick spectra are the calculated oscillator strengths, and the continuous curves are the result of convoluting these spectra with a Gaussian function (50 nm fwhm).

trans form to have the larger dipole moment, which would additionally favor this isomer in solution. These results are consistent with our NMR-based observations of <5% cis isomer in $CDCl_3$ solution at room temperature in the absence of UV excitation. "Absorption spectra" of the trans and cis isomers predicted by the AM1/CI calculations are compared with experimental spectra in Figure 4. As illustrated here, the main qualitative features of the experimental spectra are reasonably reproduced by the calculations. Thus, the relative intensity of the S_1 absorption and the approximate positions of the major bands predicted are close to those observed. (Note that the wavelength scales used for the experimental and computed spectra differ by 25 nm, but this difference is roughly what would be expected for the gas-to-solution shift.) The prediction of $S_0 \rightarrow S_{n>1}$ transitions in the region near 300 nm and their oscillator strengths relative to the $S_0 \rightarrow S_1$ absorption also appear to be consistent with the experimental spectra. Finally, we note that, at least in the gas phase, the S_1 state in *trans*-DCS is separated by 3900 cm^{-1} from the next singlet state, and as illustrated by Figure 2, this separation persists to large twist angles.

IV. Solvent Dependence of the Steady-State Spectra

Representative absorption and steady-state emission spectra of DCS are provided in Figure 5. As illustrated here, both the absorption and emission of DCS exhibit some vibronic structure in nonpolar solvents such as hexane. This structure is absent in solvents of even modest polarity like isopropyl ether. But this structure does not signal any qualitative distinction between the behavior of DCS in polar and nonpolar solvents. Measurements

TABLE 3: Characteristics of Steady-State Spectra of DCS (25 °C)

no.	solvent	n_D[b]	ϵ[b]	ν_{abs}^{pk} [c,e]	$\langle\nu_{abs}\rangle$[c,e]	ν_{em}^{pk} [c,e]	$\langle\nu_{em}\rangle$[c,e]	ν_{abs}^{0} [d,e]	Γ_{abs}[d]	S_{abs}[d]	ν_{em}^{0} [d,e]	Γ_{em}[d]	S_{em}[d]
1	*n*-hexane	1.372	1.88	26.59	26.92	23.63	22.72	25.25 ± .05	1.53	1.27	24.14 ± .05	1.17	1.26
2	cyclohexane	1.424	2.02	26.38	26.75	23.44	22.53	25.02 ± .05	1.53	1.30	23.95 ± .05	1.15	1.26
3	*n*-decane	1.410	1.99	26.37	26.74	23.47	22.57	25.04 ± .05	1.52	1.27	23.97 ± .05	1.16	1.25
4	TCTFE[a]	1.356	2.41	26.57	26.84	22.84	22.17	25.10 ± .05	1.69	1.33	23.44 ± .05	1.49	1.16
5	diisopropyl ether	1.366	3.88	26.36	26.62	21.56	21.21	24.82 ± .05	1.82	1.37	22.15 ± .14	2.01	0.97
6	ethyl acetate	1.370	6.02	26.21	26.46	20.31	20.03	24.50 ± .09	1.96	1.48	20.63 ± .28	2.33	0.68
7	tetrahydrofuran	1.405	7.58	25.99	26.25	20.13	19.92	24.24 ± .10	1.96	1.49	20.39 ± .32	2.60	0.63
8	HMPA[a]	1.457	29.30	25.34	25.71	18.90	18.91	23.81 ± .05	2.12	1.34	18.79 ± .53	2.96	0.21
9	acetone	1.356	20.56	26.13	26.39	19.23	19.11	24.10 ± .22	1.94	1.70	19.30 ± .43	2.70	0.39
10	dimethyl sulfoxide	1.478	46.45	25.37	25.74	18.31	18.20	23.52 ± .15	2.06	1.58	18.36 ± .42	2.68	0.38
11	dimethylformamide	1.428	36.71	25.64	25.97	18.62	18.50	23.83 ± .13	2.08	1.55	18.71 ± .41	2.66	0.43
12	acetonitrile	1.342	35.94	26.12	26.32	18.78	18.66	24.23 ± .15	2.13	1.58	18.85 ± .43	2.72	0.39
13	methanol	1.327	32.66	26.20	26.39	18.76	18.65	24.11 ± .24	1.99	1.74	18.86 ± .42	2.87	0.45
14	ethanol	1.359	24.55	26.09	26.32	19.15	19.06	24.14 ± .19	1.99	1.64	19.26 ± .43	2.89	0.43
15	1-propanol	1.384	20.45	26.01	26.27	19.36	19.22	24.10 ± .17	1.96	1.62	19.46 ± .42	3.01	0.48
16	1-pentanol	1.407	13.90	25.93	26.22	19.66	19.53	24.06 ± .16	1.93	1.60	19.69 ± .45	3.24	0.44
17	p-dioxane	1.420	2.21	26.23	26.51	21.21	20.87	24.52 ± .10	1.83	1.49	21.56 ± .24	2.29	0.76

[a] Solvent abbreviations are TCTFE = 1,1,2-trichlorotrifluoroethane and HMPA = hexamethylphosphoramide. [b] Values of the refractive index n_D and dielectric constant ϵ are from ref 81. [c] ν_x^{pk} and $\langle\nu_x\rangle$ are the peak and first-moment frequencies of the spectra (x = absorption or emission). [d] ν_x^0, Γ_x, and S_x are the parameters obtained from fits to the semiclassical model described by eqs 2 and 3 (with $\Gamma_x = (8 \ln 2)^{1/2}\sigma_x$). All frequencies and width parameters are in units of 10^3 cm^{-1}. [e] To avoid contributions due to additional absorption bands ($S_0 \rightarrow S_{n>1}$) at higher frequencies, the integrations required for the determination of $\langle\nu_{abs}\rangle$ were performed up to 30 000 cm^{-1}, and the fits to eqs 2 and 3 only included frequencies somewhat lower than this value. Uncertainties in ν_x^{pk} and $\langle\nu_x\rangle$ are expected to be less than 100 cm^{-1}. The uncertainties listed for the values of ν_x^0, which are used in later fitting, are estimates of the net uncertainty in determining the correct solvent-induced component of the frequencies. They are often much larger than the former uncertainties due to the ambiguity introduced by the changing band shapes.

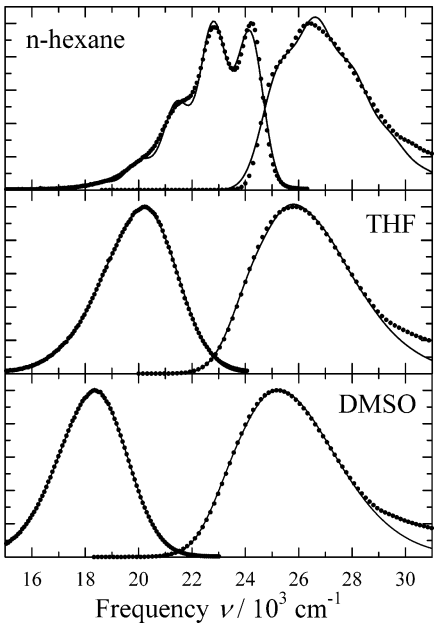

Figure 5. Steady-state absorption and emission spectra of DCS in *n*-hexane, tetrahydrofuran (THF), and dimethyl sulfoxide (DMSO). All spectra are shown normalized to constant peak height. The points denote the experimental spectra (thinned for clarity), and the solid curves are the fits to eqs 2 and 3.

in hexane + isopropyl ether mixtures (see the Supporting Information) reveal that the change in band shape from nonpolar to polar solvents is a continuous function of solvent polarity. As illustrated by the data in Figure 5, with increasing solvent polarity, both the absorption and emission bands shift to the red and simultaneously the absorption broadens whereas the emission narrows.

We have used a number of metrics to characterize the spectra of DCS in different solvents. Some of these data are collected in Table 3. Listed here are the peak ν_x^{pk} and average (first-moment) $\langle\nu_x\rangle$ frequencies measured directly from the spectra, as well as parameters derived from fitting the spectra to empirical line shape functions defined by

$$A_{abs}(\nu) \propto \nu \sum_{m=0}^{\infty} \frac{S_{abs}{}^m e^{-S_{abs}}}{m!} \exp\left\{\frac{-(h\nu_{abs}{}^0 + m\hbar\omega - h\nu)^2}{2\sigma_{abs}{}^2}\right\} \quad (2)$$

$$F_{em}(\nu) \propto \nu^3 \sum_{m=0}^{\infty} \frac{S_{em}{}^m e^{-S_{em}}}{m!} \exp\left\{\frac{-(h\nu_{em}{}^0 - m\hbar\omega - h\nu)^2}{2\sigma_{em}{}^2}\right\} \quad (3)$$

These expressions represent each spectrum by a progression of vibronic peaks of width $\Gamma = (8 \ln 2\sigma)^{1/2}$ built on a "0−0 frequency" ν^0 and resulting from a single harmonic mode of frequency ω displaced by an amount $\Delta = (2S)^{1/2}$. Expressions of this sort can be derived from a semiclassical description of electronic spectra[43] in which case classical reorganization terms would be separated from the $h\nu^0$ terms and explicitly connected to the widths of the vibronic lines σ (or Γ). Here, we use eqs 2 and 3 to provide both well-defined frequencies for solvatochromic analysis and approximate measures of how the vibronic structure changes with solvent, via the Huang−Rhys factor S. The curves in Figure 5 show fits of the experimental data (points) using these expressions. As illustrated in this figure, the fit is good in nonpolar solvents such as hexane and excellent in more polar solvents. Furthermore, by fixing the vibrational frequency ω at the value observed in hexane (1375 cm^{-1}) when fitting all other spectra, both absorption and emission, we find that the remaining spectral parameters are precisely defined by these fits. Note that, as predicted by the calculations of the last section, there appears to be an additional absorption due to $S_0 \rightarrow S_{n>1}$ transitions in the region $\nu > 28\,000$ cm^{-1}. This region is therefore excluded when fitting the absorption spectra.

The absorption and emission frequencies of DCS are well correlated by dielectric measures of solvent polarity, as has already been noted in several previous reports.[9−11] An example of such a correlation is provided in Figure 6 where we plot ν_{abs}^0 and ν_{em}^0 vs the dielectric function $d_c(\epsilon) - d_c(n_D{}^2)$ where ϵ and

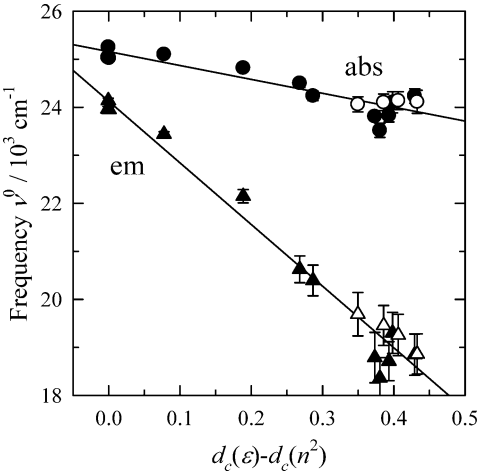

Figure 6. Absorption and emission "0−0" frequencies plotted against the dielectric continuum measure of solvent nuclear polarizability $d_c(\epsilon) - d_c(n^2)$. Circles and triangles denote absorption and emission frequencies and filled and open symbols denote polar aprotic and alcoholic solvents, respectively. The data for dioxane is not included in this figure due to the inability of dielectric models to properly capture the polarity of this quadrupolar solvent.[72]

n_D are the solvent dielectric constant and refractive index and

$$d_c(x) \equiv \frac{d_0(x)}{1 - 2cd_0(x)} \quad \text{with} \quad d_0(x) \equiv \frac{x-1}{2x+1} \tag{4}$$

As described shortly (and in detail in the Appendix), the function $d_c(\epsilon) - d_c(n_D^2)$ represents the nuclear solvent response to a polarizable dipolar solute. The solute polarizability operates through the factor c, for which we use a value of 0.235. We will discuss the choice of this value and the interpretation of these correlations further in section VI. For now, we merely concentrate on empirically describing the solvent dependence observed in the spectra. In Figure 6, we distinguish between polar aprotic solvents (filled symbols) and alcohols (open symbols). As illustrated in this figure, there is no distinction between the behavior of DCS in these two solvent classes. The same can also be said of all of the other equilibrium photophysical properties we have examined.

Other characteristics of the spectra (i.e., Γ and S) can also be correlated to dielectric measures of solvent polarity. However, it is probably best to view these other quantities as being primarily connected to the observed frequencies. These relationships are illustrated in Figure 7. The correlations displayed in this figure show that the widths (Γ) of the individual vibronic bands in absorption and emission increase at comparable rates as solvent polarity increases and the spectra shift to the red. The Huang−Rhys factors S_{abs} and S_{em}, which describe the breadth of the vibronic progression (or the reorganization energy in the high-frequency mode, $\lambda_{vib} = \hbar\omega S$), change in opposite directions as the spectra shift. The relative change in S_{em} between nonpolar and highly polar solvents is nearly a factor of 3, and this change leads to the overall narrowing of the emission spectra with increasing solvent polarity. The origins of these changes will be considered in section VI B.

V. Transition Dipole Moments

Significant differences between the character of the electronic states responsible for absorption and emission, or variations in the character of these states with solvent polarity, should be clearly revealed in the transition dipole moments coupling S_0 and S_1. For this reason, we have measured the absorption and emission transition dipole moments of DCS in several solvents. The data required are compiled in Table 4, together with available comparisons of data from previous studies. We note that the extinction coefficients ϵ_{max} and emission quantum yields ϕ_{em} measured here tend to systematically be higher than most literature values, with average differences being ∼15% in ϵ_{max} and ∼60% in ϕ_{em}. In contrast, our emission lifetimes τ_{em} are in excellent agreement with literature values. We conjecture that these differences in the former quantities but not in τ_{em} might reflect the effects of cis photoproduct contamination, which, as described in the Experimental Methods section, has the largest effect on ϕ_{em} measurements but is undetectable in the emission decays.

Absorption transition moments are calculated according to the relation[44,45]

$$M_{abs}^{\ 2} = \frac{3hc}{8\pi^3}\frac{\ln(10)}{N_A}\frac{1}{f(n)}\frac{1}{n}\int_{abs}\frac{\epsilon(\nu)}{\nu}\,d\nu \tag{5}$$

where h is Planck's constant, c the speed of light, N_A Avogadro's number, n the solvent refractive index, and $\epsilon(\nu)$ the decadic molar extinction coefficient. The integration over $\epsilon(\nu)$ is taken from a low value of ν to the minimum in $\epsilon(\nu)$ near 31 000 cm^{-1} (see Figure 5). Emission transition moments are calculated from[44,45]

$$M_{em}^{\ 2} = \frac{3hc^3}{64\pi^4}\frac{1}{f(n)}\frac{k_{rad}}{n^3\tilde{\nu}^3} \tag{6}$$

where $\tilde{\nu}^3 = \int F(\nu)\,d\nu / \int F(\nu)\nu^{-3}\,d\nu$ with $F(\nu)$ denoting the observed emission spectrum and $k_{rad} = \phi_{em}/\tau_{em}$. The factor $f(n)$ appearing in both of these expressions is a reaction field factor relating the external electric field to the "internal" field acting on the molecule. There are varying opinions as to the correct form of $f(n)$.[46−48] For simplicity, we adopt the choice $f(n) = 1$.[44] As shown in previous work,[45] popular alternative choices of $f(n)$ do not alter the solvent dependence of the calculated moments significantly, but they tend to uniformly increase the transition moments calculated by up to 17%.

At least to within the appreciable uncertainties in these data, both the absorption and emission transition moments are independent of solvent and nearly equal:

$$M_{abs} = 6.7 \pm 0.4\ \text{D} \quad \text{and} \quad M_{em} = 7.6 \pm 0.8\ \text{D}$$

Thus, we find no evidence for any marked variation in the nature of the S_1 state as a function of solvent polarity. The fact that M_{abs} and M_{em} are nearly equal also argues against there being a substantial difference between the Franck−Condon state reached by absorption and the state from which emission occurs. Finally, given the near-zero transition moments predicted for the anilino TICT state in the previous section, and the large transition moments observed here ($f \sim 1$ in all solvents), it is unlikely that such a state plays any significant role in the observed emission of DCS.

VI. Modeling the Solvent Dependence of the Spectra

We now attempt to analyze the solvent dependence described in the last two sections, to learn what these data imply about the electronic states of DCS in solution. We consider two different models. Both models employ a relatively standard description of solute−solvent interactions, treating the solute as a spherical cavity of radius a containing a point dipole moment and some sort of polarizability and the solvent as a dielectric continuum. In the first model, we assume that all of

TABLE 4: Quantities Related to Transition Dipole Moment Determinations[a]

no.	solvent	$\epsilon_{max}/10^3$ M^{-1} cm^{-1}	ϕ_{em}	τ_{em}/ps	k_{rad}/ns^{-1}	k_{nr}/ns^{-1}	M_{abs}/D	M_{em}/D
1	*n*-hexane		0.040	65	0.62	15		8.2 ± 1
2	cyclohexane	33 (28[e])	0.050 (0.03[b],0.06[g])	75 (75[d],66[g])	0.67	13	6.0 ± .2	8 ± 2
3	*n*-decane		0.052	87	0.59	11		7.8 ± 1
5	isopropyl ether	37 (29[h,i])	0.043	101	0.42	9.5	6.7 ± .2	7.6 ± 1
7	tetrahydrofuran	37 (36[b,c])	0.10 (0.06[b,c])	242	0.43	3.7	6.8 ± .2	8.0 ± .8
10	dimethyl sulfoxide		0.26 (0.11[d])	937 (900[d])	0.28	0.8		6.9 ± .5
11	dimethylformamide		0.19 (0.13[b])	667	0.29	1.2		7.2 ± .6
12	acetonitrile	37 (31[h])	0.17 (0.13[b],0.15[f],0.11[g])	507 (507[f])	0.33	1.6	7.1 ± .2	8.4 ± .8
13	methanol	34	0.14	445 (435[f])	0.30	1.9	7.0 ± .2	8.2 ± .6
15	1-propanol	34	0.11	345 (332[f])	0.30	2.6	6.7 ± .2	7.3 ± 2
16	1-pentanol		0.069	338	0.20	2.8		5.7 ± 1

[a] ϵ_{max} denotes the maximum value of the decadic molar extinction coefficient, ϕ_{em} and τ_{em} the emission quantum yield and lifetime, k_{rad} and k_{nr} the radiative and nonradiative rate constants, and M_{abs} and M_{em} the absorption and emission transition dipole moments. Uncertainties in these quantities are estimated to be roughly 5% of ϵ_{max}, 5−15% of ϕ_{em}, and ∼5% of τ_{em}. Values in parentheses are from the literature sources: [b] Reference 12. [c] The solvent used was methyltetrahydrofuran rather than tetrahydrofuran. [d] Reference 2. [e] Reference 11. [f] References 10 and 13. [g] Reference 82. [h] Reference 9. [i] The solvent used was ethyl ether rather than isopropyl ether.

TABLE 5: Results of Fitting ν_{abs} and ν_{em} to Various Models[a]

5A. Dielectric Regressions

	χ_ν^2	#ν	ν^0_{abs}	A_{abs}	C_{abs}	ν^0_{em}	A_{em}	C_{em}
R1	6.4	4	25.16	(0)	−2.89	24.13	(0)	−12.84
R2	1.0	6	27.70	−12.00	−2.98	28.07	−18.61	−12.97

5B. Fits to the Complete Independent-State Model

	χ_ν^2	#ν	ΔF^0	λ_{vib}	μ_0	μ_1	α/a^3	$\mu_0(\epsilon=\infty)$	$\mu_1(\epsilon=\infty)$
F1	6.7	3	26.19	0.67	(7.5)	18.0	(0.24)	9.8	23.5
F2	4.7	3	26.65	0.62	(7.5)	21.0	(0)	7.5	21.0
F3	1.6	4	26.25	0.54	4.2	17.5	(0.24)	5.5	22.8
F4	0.8	5	25.66	0.55	3.1	13.1	0.55	2.2	29.1

5C. Fit to Coupled-State Model

	χ_ν^2	#ν	ΔE	Λ_{vib}	V_{el}	μ_N	μ_{CT}		χ_0	χ_1	μ_0	μ_1	α_0/a^3	α_1/a^3
CS	3.3	4	20.9	3.39	8.3	(0)[b]	23.9	$\epsilon=1$	0.91	0.87	2.2	20.8	0.09	−0.14
								$\epsilon=\infty$	0.88	0.75	2.9	17.8	0.13	−0.30

[a] χ_ν^2 is the goodness-of-fit parameter, and #ν is the number of model parameters varied in the fit. Other quantities are described in the text. Energetic quantities ν_x^0, ΔF^0, λ_{vib}, ΔE, Λ_{vib}, and V_{el} are in units of 10^3 cm^{-1}, dipole moments are in units of Debye, and the regression slopes A_x and C_x are in units of 10^3 cm^{-1} Å^3 D^{-2}. Values in parentheses indicate parameters held constant in a given fit. In all cases, the solute cavity radius is fixed at a value of $a = 5.75$ Å. [b] Because the electronic polarizabilities vary little among the solvents studied, the predictions of the CS model are primarily dependent on the difference dipole $\mu_{CT} - \mu_N$ rather than on their individual values. For simplicity, we therefore fixed $\mu_N = 0$.

the relevant properties of the solute, the cavity radius, the (gas-phase) dipole moments $\vec{\mu}_0$, $\vec{\mu}_1$ in the S_0 and S_1 states, and the polarizability α, are independent of the solvent. We will refer to this model as the "independent-state" ("IS") model. Such a model is at least partially successful in interpreting the spectral shifts observed, however, it is an incomplete description regarding transition moments and is also mute as to why the vibronic structure in emission should charge so markedly with polarity.

We therefore also consider the experimental data in light of a description in which the properties of the S_0 and S_1 states are assumed to derive from solvent-dependent mixing between two valence bond states of differing charge-transfer character. This model has the advantage over the IS model that it allows for a more proper description of transition moments and an initial treatment of vibronic struture. We refer to this second model as the coupled-state ("CS") model. Both models are explained in detail in the Appendix. Here, we focus on their ability to represent the experimental observations.

A. Independent-State (IS) Model. In the IS model, the electronic properties important to solvatochromism, a, $\vec{\mu}_0$, $\vec{\mu}_1$, and α, are considered to be characteristics of the isolated solute and to be independent of the solvent. This type of model is most often used to derive solute dipole moments from solvatochromic data of the sort shown in Figure 6. In first pass, we take the polarizabilities of the two states to be fixed at the value $0.235a^3$ estimated from semi-empirical calculations in a continuum solvent.[49] As detailed in the Appendix, such a model predicts that the absorption and emission frequencies should be linearly related to the reaction field functions $d_c(x)$ defined in eq 4 via

$$h\nu_{abs} = h\nu_{abs}{}^0 + A_{abs}d_c(n^2) + C_{abs}\{d_c(\epsilon) - d_c(n^2)\} \quad (7)$$

$$h\nu_{em} = h\nu_{em}{}^0 + A_{em}d_c(n^2) + C_{em}\{d_c(\epsilon) - d_c(n^2)\} \quad (8)$$

where

$$A_{abs} = -(\mu_1{}^2 - \mu_0{}^2)a^{-3} \quad C_{abs} = -2\mu_0(\mu_1 - \mu_0)a^{-3} \quad (9)$$

$$A_{em} = -(\mu_1{}^2 - \mu_0{}^2)a^{-3} \quad C_{em} = -2\mu_1(\mu_1 - \mu_0)a^{-3} \quad (10)$$

and where $c = \alpha/a^3$ (0.235 here). In eqs 9 and 10 and in the subsequent discussion, we assume that $\vec{\mu}_0$ and $\vec{\mu}_1$ are parallel, which is an excellent approximation according to electronic structure calculations (Figure 1).

Table 5A lists the results of fitting the "0−0" frequencies according to eqs 7−10. The first row "R1" provides the constants of the lines plotted in Figure 6, which is the fit obtained by ignoring the dependence on $d_c(n^2)$ in these equa-

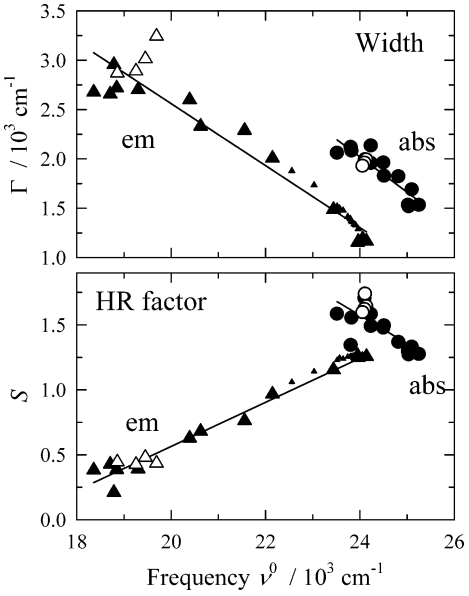

Figure 7. Correlations of the width of individual vibronic bands (Γ) and the Huang−Rhys factor (*S*) in the absorption and emission spectra with the spectral frequency. All of these spectral characteristics are obtained from fits of the spectra according to eqs 2 and 3. Large points denote data in pure solvents, with filled symbols for aprotic solvents, and open symbols denote protic solvents. Small filled triangles are emission data from a series of 18 *n*-hexane + isopropyl ether mixtures. The correlation lines shown here are $\Gamma_{abs} \cong 10.62-0.358\nu^0_{abs}$, $\Gamma_{em} \cong 8.84-0.314\nu^0_{em}$, $S_{abs} = 6.80-0.218\nu^0_{abs}$, and $S_{em} = -2.83 + 0.169\nu^0_{em}$.

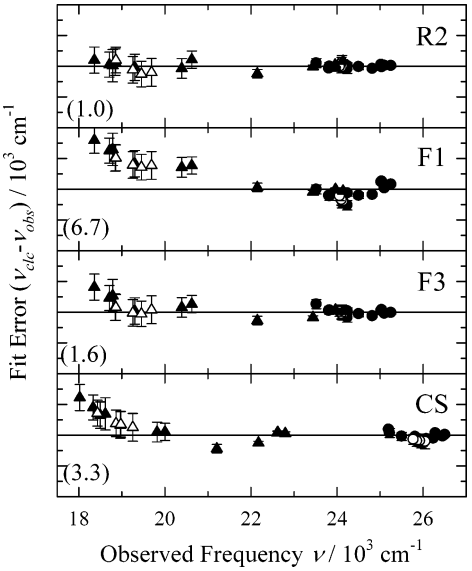

Figure 8. Errors in frequencies ν_{abs} (circles) and ν_{em} (triangles) calculated according to various models. From top to bottom the fits shown correspond to regression #2 ("R2" in Table 5A), fits 1 and 3 to the independent-state model ("F1" and "F3" in Table 5B), and the fit to the coupled-state model ("CS" Table 5C). The vertical scale of each panel spans the range of ±2000 cm^{-1}. The values of the goodness-of-fit parameter χ_ν^2 are indicated in parentheses. Note that the frequencies fit in the top three panels are apparent 0−0 frequencies ν^0 whereas peak frequencies ν^{pk} are used in the bottom panel. Filled symbols denote aprotic solvents, and open symbols denote protic solvents.

tions. The quality of this fit can be judged by the goodness-of-fit parameter χ_ν^2, which should be close to unity if the model represents the experimental data to within its estimated uncertainties.[50,51] The value $\chi_\nu^2 = 6.4$ here indicates, as does inspection of Figure 6, that the data cannot be fit to within the estimated uncertainties in this manner. Inclusion of the electronic polarizability term (fit "R2" in Table 5A) leads to a greatly improved fit, as indicated by the value $\chi_\nu^2 = 1.0$. Although addition of this term does not alter the slopes C_{abs} and C_{em} significantly, it greatly reduces the deviations from the basic trend with $d_c(\epsilon) - d_c(n^2)$ shown in Figure 6. The top panel of Figure 8, which shows the deviations between calculated and observed frequencies, illustrates the good quality of this latter fit.

Unfortunately, the coefficients derived from these regressions do not provide a consistent description of the dipole moments of DCS within the context of the above model. If one assumes the dipole moment in S_0 and the cavity radius to be known, all four parameters A_{abs}, C_{abs}, A_{em}, and C_{em} can be used to estimate the dipole moment of the S_1 state. For example, adopting the value $\mu_0 = 7.5$ D, which is a compromise between the experimental and calculated dipole moments (Table 1), and the value $a = 5.75$ Å, based on the estimated van der Waals volume of DCS,[52] the best determined coefficients C_{abs} and C_{em} indicate S_1 dipole moments of $\mu_1 = 15.0 \pm 0.2$ and 19.8 ± 0.0 D, respectively. The difference between these two estimates is well beyond the uncertainties in the data. Using a similar sort of analysis, Zachariasse and co-workers[10] previously concluded that there must be a significant difference between the dipole moment of DCS in the Franck−Condon state created by absorption ($\mu_1^{FC} \sim 15$ D from C_{abs}) and that of the equilibrated emitting state ($\mu_1^{eq} \sim 20$ D). We consider this idea further after presenting a more complete analysis using the same basic model.

To explore whether the discrepancy noted above is a result of simplifications made in deriving eqs 6−9 or is due to particular choices of model parameters, we also fit the experimental frequencies directly to the full IS model using a nonlinear least-squares approach. Calculating ν_{abs} and ν_{em} using this representation of a polarizable dipolar solute having two independent electronic states depends on the collection of six model parameters: a, ΔF^0, λ_{vib}, μ_0, μ_1, and α. In addition to the parameters already described, ΔF^0 is the free energy difference between the equilibrium S_0 and S_1 states in the gas phase and λ_{vib} is the vibrational reorganization energy associated with any low-frequency internal modes not accounted for by fitting the spectra to a single high-frequency oscillator using eqs 2 and 3. Table 5B and the panels labeled "F1" and "F3" in Figure 8 summarize the results of fitting to this full model. In all of these fits, we maintain the cavity radius fixed at the value $a = 5.75$ Å. As illustrated by eqs 7−10, frequency shifts are determined by ratios of the sort μ^2/a^3 and thus μ_0, μ_1, and a are not all independent. We therefore fix a at a value that should provide sensible magnitudes of the dipole moments.[10,52]

The first fit, labeled "F1" in Table 5B, is one in which only ΔF^0, λ_{vib}, and μ_1 are allowed to vary, while anticipated values of $\mu_0 = 7.5$ D and $\alpha \cong 0.24a^3$ are specified for the remaining model parameters. This fit yields a value of $\chi_\nu^2 = 6.7$, which shows it to be of comparable quality to the four-parameter regression R1. Large systematic errors in both ν_{abs} and ν_{em} are found with this fit. A slightly better, but still unacceptable fit (F2 in Table 5B), is achieved when the solute is assumed to be nonpolarizable ($\alpha = 0$). This is the choice made in previous solvatochromic modeling.[10,11,14] When comparing the polarizable and nonpolarizable results, it is important to note that the model dipole moments μ_0 and μ_1 discussed here are gas-phase values. The effective dipole moments in solution are larger by a factor of $[1 - 2(\alpha_i/a^3)d_0(\epsilon)]^{-1}$ when the solute is polarizable.[42] For comparison purposes, the final columns in Table 5B list the limiting $\epsilon \rightarrow \infty$ values of the effective solution-phase dipole moments. The remaining two fits (F3 and F4) in Table 5B

illustrate the effects of allowing μ_0 and α to vary. Good agreement with experiment, $\chi_\nu^2 = 1.6$ if the four parameters are varied and $\chi_\nu^2 = 0.8$ if five parameters are varied, can be achieved only when the ground-state dipole moment is allowed to take on values that are considerably smaller than those expected.

B. Coupled-State (CS) Model. We next consider the experimental data in terms of a coupled two-state description of the spectroscopy. In this description, rather than the S_0 and S_1 states being of fixed character, they are described in terms of the mixing of two valence states of markedly different polarities, denoted "N = neutral" and "CT = charge transfer". Solvent-dependent modulation of the energy gap between the N and CT states results in a variable mixing and thus variations in the properties of the resulting S_0 and S_1 states with solvent. Such models have a long history in the context of charge-transfer spectroscopy[53,54] and a number of recent papers have discussed such models.[5,46,55−63] The details of the particular version we employ are described in the Appendix. It includes a vibrational displacement between the N and CT states in the manner recently proposed by Matyushov and Newton[63] and Painelli and co-workers[59−61] for exploring the relationship between solvation and vibronic structures.

The six parameters specifying the CS model are the solute cavity radius *a*, the gas-phase energy gap ΔE, the electronic coupling V_{el} between the N and CT states, the dipole moments of these states, μ_N and μ_{CT} (assumed parallel), and the vibrational reorganization energy between them, Λ_{vib}. In this model, the basis states are assumed to be nonpolarizable. Mixing between these states confers polarizabilities on the S_0 and S_1 states that are of approximately the same magnitude but of opposite sign in the two states, with the polarizability of S_1 being negative. This unrealistic feature of the model could be remedied by the addition of explicit polarizabilities to each state as was done by Matyushov and Newton,[63] but we have chosen not to do so in order to maintain the simplicity of the two-state picture here.

The CS model includes an explicit vibrational coordinate whose displacement between the S_0 and S_1 states varies with the solvent. We therefore use the model to fit the peak frequencies of the absorption and emission spectra (ν^{pk} in Table 3) rather than the "0−0" frequencies ν^0 we have used thus far. Table 5C and the bottom panel of Figure 8 illustrate the best fit obtained with the CS model. The fit is of lower quality than that achieved with the IS model using the same number of adjustable parameters: $\chi_\nu^2 = 3.3$ and clear systematic trends in the residuals can be seen in Figure 8 (bottom panel). Nevertheless, the CS model provides a sensible representation of the data, similar in most respects to the IS model. For example, the electronic coupling matrix element V_{el} obtained from fitting the frequency data (8300 cm^{-1}) is close to the value $V_{el} = 9200$ cm^{-1} estimated from the AM1/CI calculations using a generalized Mulliken−Hush approach.[64] Also listed in Table 5C are properties of the S_0 and S_1 states predicted by the CS model at two extremes of solvent polarity. The quantities χ_0 and χ_1 measure the extent of N−CT mixing in the S_0 and S_1 states. The values listed here indicate that in the gas phase ($\epsilon = 1$) the equilibrium S_0 state is of 91% N character and the equilibrium S_1 state is of 87% CT character. In highly polar solvents ($\epsilon = \infty$), the extent of mixing is predicted to be significantly larger, especially in S_1. The dipole moments calculated for S_1 are close to those obtained from the IS model fits. As in the case of the IS model, the best fits of the experimental frequencies to the CS model imply values of μ_0 that are unrealistically low.

Although the CS model does not represent the frequency data as well as the IS model, it provides insight into the solvent

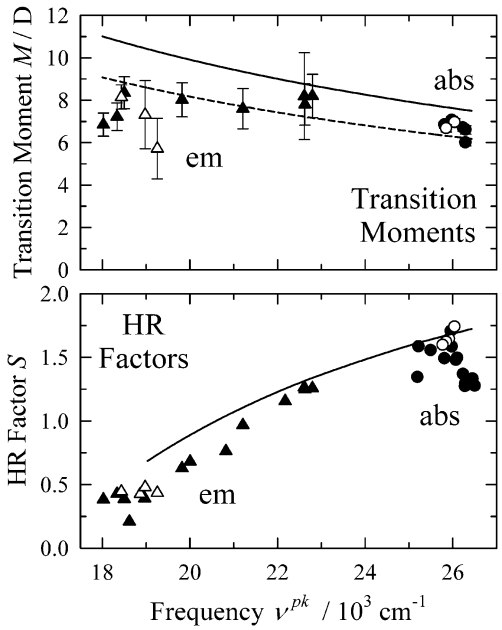

Figure 9. Observed and CS model predictions for the absorption and emission transition moments and Huang−Rhys factors plotted as functions of peak frequency. The experimental results are shown as points, with the circles being absorption and triangles the emission data. The model predictions are the solid curves. The dashed line in the top panel is the model prediction scaled by a factor of 0.8 for comparison to the experimental trend. When the Huang−Rhys factors are calculated from the CS model, a value of $\lambda_{vib} = 550$ cm^{-1}, obtained from the fits to the IS model, was subtracted from the fitted value of Λ_{vib} to account for low-frequency contributions. Filled symbols denote aprotic solvents, and open symbols denote protic solvents.

dependence found in other features of the spectra. For example, in section V we found that the transition moments of absorption and emission are approximately equal to one another and apparently invariant with solvent. This sort of behavior is what would be anticipated if the S_0 and S_1 states were truly independent, as assumed in the IS model. On the basis of this viewpoint, we previously interpreted such behavior to indicate an $S_0 \leftrightarrow S_1$ transition uncomplicated by the presence of significant interactions with other electronic states.[45] However, such a perspective has been criticized as being inconsistent[46,59] because, if only two electronic states are involved, the transition moments should be inversely proportional to the transition frequencies (eq A35) and therefore display the same solvent dependence as these frequencies. It is therefore of interest to see what the CS model, fitted to the experimental frequencies, implies about the transition moments.

A comparison of the model and experimental results is shown in the top panel of Figure 9. It is noteworthy how close the model transition moments (solid curve) are to the experimental values. Averaging over the entire set of absorption and emission data yields a calculated average of 8.8 D vs 7.2 D from experiment. This 20% average difference could easily be accounted for by choosing a different $f(n)$ function to evaluate the experimental moments (see eqs 5 and 6 and text) or a modest increase in the cavity radius employed in the model. However, the frequency dependence of the model is not reflected in the experimental data. The observed values of ν_{abs}^{pk} and ν_{em}^{pk} span the range $(18-26) \times 10^3$ cm^{-1}, and over this range, the CS model predicts a factor of 1.45 variation in the transition moments. Although the uncertainties in the emission transition moments are large (and there may be systematic errors in correction factors not accounted for here), the data do not seem

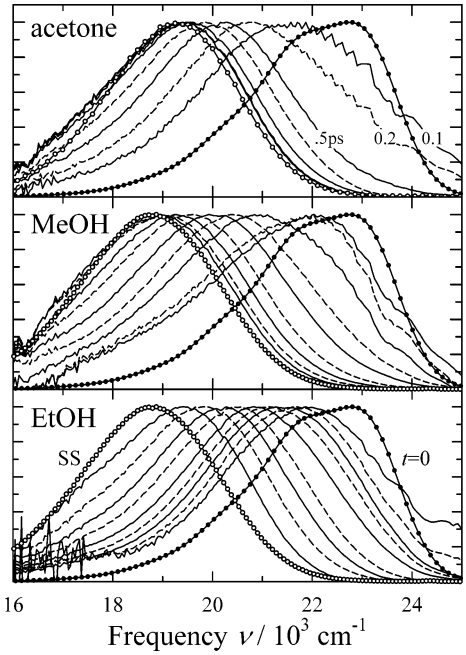

Figure 10. Representative time-resolved spectra in acetone, methanol, and ethanol. These spectra are the result of iterative reconvolution fitting and spectral correction of the raw data. Peak-normalized spectra are plotted at times of 0.1, 0.2, 0.5, 1, 2, 5, 10, 20, and 50 ps from right to left. Solid and dashed lines are used for alternating times for clarity. The spectra marked with filled symbols are the estimated time-zero spectra, and those with open symbols are the steady-state spectra.

to support such a large variation. It is more likely that the two-state representation used here is oversimplified and that there is some modest mixing of S_1 with other states that accounts for the discrepancy, as has been suggested in other cases.[47,65,66]

The CS model also predicts a dependence of the vibronic line widths, as represented by the Huang−Rhys factors S_{abs} and S_{em}, upon transition frequency. The comparison between the model predictions and experiment is provided in the bottom panel of Figure 9. A much stronger frequency dependence is predicted for these quantities than for the transition moments, and this dependence is rather close to what is observed in experiment. In viewing the comparisons in Figure 9, it should be emphasized that the predictions of both M_x and S_x have been made solely on the basis of the model parameters required to fit the experimental frequencies. No further adjustment is made here. Furthermore, only four quantities, ΔE, V_{el}, $(\vec{\mu}_{CT} - \vec{\mu}_N)/a^3$, and Λ_{vib} are important in determining these results. The level of agreement shown for both M_x and S_x is therefore a strong endorsement of the utility of this coupled-state approach as a starting point for understanding the spectroscopy of DCS. The systematic deviations in the frequencies shown in Figure 8, as well as the incorrect frequency dependence predicted for M_{em}, suggest that refinement of the model, by incorporating the effects of mixing additional states with S_1, might prove fruitful. But we leave such refinements to future work.

VII. Time-Dependent Emission Spectra

We have measured time-resolved emission spectra of DCS in 13 solvents using the Kerr-gated emission method.[34] Representative spectra in three solvents are shown in Figure 10. These spectra were derived by fitting the raw decay data with an iterative reconvolution scheme[34] to partially remove the effects of instrumental broadening. (The instrumental response here is 450 fs fwhm.) Also shown in Figure 10 are the steady-state spectra (open circles) and the spectra expected prior to any solvent relaxation (filled circles). The latter, "time-zero" spectra were generated using eq 3 by assuming that $\nu^0_{em}(t = 0) \cong \nu^0_{abs} - 2\lambda_{vib}$ and using the steady-state correlations in Figure 7 to estimate the line shape parameters via $\Gamma_{em}(t = 0) \cong \Gamma_{em}[\nu^0_{em}(0)]$ and $S_{em}(t = 0) \cong S_{em}[\nu^0_{em}(0)]$. As illustrated by the data in Figure 10, the early time-resolved spectra appear to extrapolate reasonably to these estimates of the initial spectra. In the highly polar solvents depicted here, the magnitude of the dynamic Stokes shift is about 3000 cm^{-1}. It decreases to $\sim$1000 cm^{-1} in the least polar solvent examined, diisopropyl ether (Table 6). The spectral evolution in all cases consists primarily of a continuous spectral shift, without dramatic changes in spectral shape or intensity. We sometimes observe irregularities in the shapes and widths of the early-time spectra of the sort exemplified by the acetone data in Figure 10. These irregularities are not reproducible and are mainly related to difficulties in completely removing the effects of Raman scatter near 24 000 cm^{-1} from the spectra. These spectra do not indicate the presence of the sort of two-state kinetics that was previously suggested for DCS in acetonitrile,[31] methanol,[31] and ethanol.[29] Our observations are instead consistent with the more recent conclusion of Ernsting and co-workers[28] that solvation dynamics is entirely responsible for the observed spectral evolution.

To analyze these data further, we determined the time dependence of the average (first-moment) frequencies of the spectra $\bar{\nu}(t)$ by performing simultaneous iterative reconvolution fits of the zeroth and first moments of the raw spectra.[34,67] The main results of this analysis are summarized in Table 6. Figure 11 shows examples of the deconvoluted $\bar{\nu}(t)$ data in the form of normalized spectral response functions

$$S_\nu(t) = \frac{\bar{\nu}(t) - \bar{\nu}(\infty)}{\bar{\nu}(0) - \bar{\nu}(\infty)} \tag{11}$$

The solid curves in Figure 11 are what is observed with DCS. Also shown for comparison are data recorded previously[68] with the well-established solvation probe coumarin 153 (C153).[45,68−72] The latter data were obtained using a fluorescence upconversion instrument with a 120 fs response time. As illustrated by these comparisons, the normalized spectral dynamics of DCS are comparable to those of C153. Both the time scale of the relaxation and, as illustrated here, the shapes of the $S_\nu(t)$ response are similar in these two solutes.

A more complete comparison of the $S_\nu(t)$ dynamics of DCS and C153 is provided in Figure 12. Here, we plot two characteristic times of the response functions, the 1/*e* time (t_{1e}) and integral time ($\langle t \rangle$) in 11 solvents. Figure 12 shows that the solvent variations in the spectral response times of the two solutes are strongly correlated over more than two decades. In the case of C153, numerous studies have shown that $S_\nu(t)$ provides a reliable measure of the solvation response to the charge redistribution accompanying the $S_0 \rightarrow S_1$ transition.[68,71−75] The present comparison suggests that the spectral dynamics in DCS likewise monitor polar solvation dynamics. To within combined uncertainties, the solvation times measured by the two solutes are equal in polar aprotic solvents (filled symbols). In alcohol solvents, the times measured by DCS appear to be systematically shorter than those of C153, on average by a factor of nearly 2. This difference may indicate a difference in the way specific hydrogen bonding influences the dynamics in the two solutes, and it would be interesting to explore this difference further in future work. For now, however, we take the close parallel between the behavior of DCS and C153 in a variety of solvents as a clear indication that the primary dynamics reflected

TABLE 6: Summary of Stokes Shift Dynamics (20 ± 1 °C)[a]

no.	solvent	$\nu_{em}/10^3$ cm^{-1} [b]	$\nu(\infty)/10^3$ cm^{-1} [b]	$\Delta\nu$(est)/10^3 cm^{-1} [c]	$\Delta\nu$(obs)/10^3 cm^{-1} [d]	t_{1e}/ps [e]	$\langle t\rangle$/ps [e]
5	diisopropyl ether	21.21	21.35	1.22	1.31	4.4	4.5
6	ethyl acetate	20.03	20.10	2.17	2.10	1.3	1.5
7	tetrahydrofuran	19.92	19.84	2.09	1.82	0.94	1.0
8	HMPA	18.91	18.70	2.28	3.51	7.8	11
9	acetone	19.11	19.16	2.79	2.97	0.43	0.48
10	dimethyl sulfoxide	18.20	18.44	3.23	2.73	0.83	1.6
11	dimethylformamide	18.50	18.61	3.18	2.67	0.79	1.1
12	acetonitrile	18.66	18.77	3.33	3.58	0.08	0.37
13	methanol	18.65	18.86	3.25	3.20	1.0	2.5
14	ethanol	19.06	19.00	2.86	2.96	7.0	13
15	1-propanol	19.22	19.30	2.68	2.75	13	20
16	1-pentanol	19.53	19.45	2.34	2.95	24	54
17	p-dioxane	20.87	20.95	1.33	1.37	1.4	1.9

[a] All frequencies here are first spectral moments, $\int F(\upsilon)\nu\, d\nu / \int F(\upsilon)\, d\nu$. [b] ν_{em} values are from the steady-state spectra ($\langle\nu_{em}\rangle$ in Table 3), and $\nu(\infty)$ values are the apparent infinite time frequencies obtained by fitting the time-resolved spectra. [c] $\Delta\nu$(est) is the estimated magnitude of the solvation Stokes shift based on the difference between the average frequencies of the estimated time-zero spectra described in the text and the steady-state spectra. [d] $\Delta\nu$(obs) is the value obtained by fitting the time-resolved spectra. [e] t_{1e} and $\langle t\rangle$ are the 1/*e* and integral times of the normalized spectral response. Uncertainties in these times are estimated to be roughly ±20% except for HMPA (±40%) and pentanol (±35%).

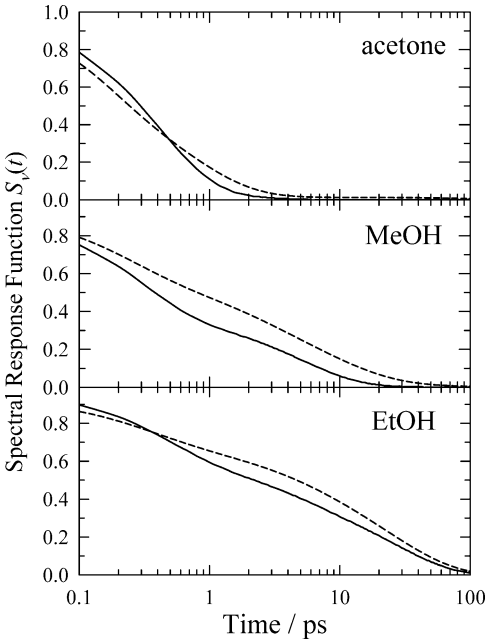

Figure 11. Comparison of spectral response functions of DCS obtained here (solid) and those of C153 obtained from prior work[68] (dashed) in acetone, methanol, and ethanol. The DCS response functions were obtained using the KGE technique and the average frequencies obtained by first-moment deconvolution (see text), whereas the C153 functions were obtained from log-normal fits to reconstructed spectra.

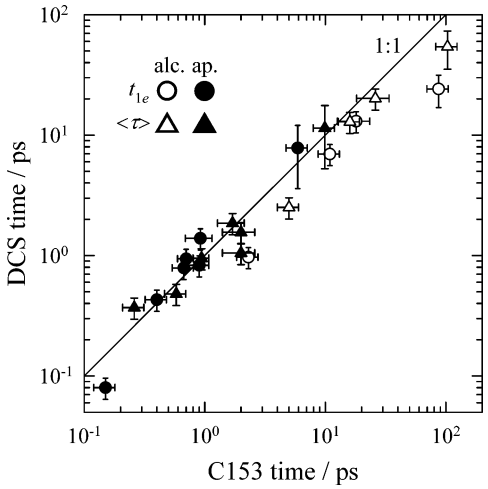

Figure 12. Comparison of characteristic times t_{1e} (circles) and $\langle t\rangle$ (triangles) of the spectral response functions of DCS and C153[68] in 11 solvents. Aprotic solvents are denoted by filled symbols, and alcohols are denoted by open symbols.

in the time-dependent emission of DCS is also the polar solvation response.

VIII. Summary and Conclusions

The primary aim of this work was to survey the solvent dependence of the electronic spectroscopy and emission dynamics of DCS, with a view toward clarifying the much debated nature of its S_1 state. Electronic structure calculations, performed as a preliminary to the experimental work, mainly served to reinforce conclusions of previous theoretical studies.[4,14−20,28] They showed the $S_0 \rightarrow S_1$ transition to entail a sizable (>0.25 *e*) shift of charge from the anilino ring to the remainder of the molecule. As in previous studies,[14,16,17] the present calculations show that a similar transfer, but of a full electronic charge, takes place in a higher lying (S_5) excited state upon twisting the anilino bond by 90°. Although this TICT state lies much higher in energy than S_1 in the gas phase, in polar solvents, its large dipole moment (>30 D) would be expected to reduce its energy to near if not below that of $S_1(0°)$. Thus, as in previous calculations with other methods, the idea that emission might occur from a TICT state in polar solvents[16,17,23,30] is supported by the present AM1/CI calculations. However, what was not stressed in previous work is the fact that this S_5 state is calculated to have a very small transition moment with S_0 for any anilino twist angle, and this transition moment drops to virtually zero at the 90° TICT state.

The magnitudes of the absorption and emission transition moments of DCS measured here clearly rule out participation of such a TICT state. In a variety of solvents, we find the absorption transition moments all fall in the range 6.7 ± 0.4 D and emission moments in the range 7.6 ± 0.8 D. These transition moments are large and to within uncertainties independent of solvent. In addition to eliminating the possibility of emission from a TICT state, the transition moment data also argue against any large change in the composition of the S_1 state, either with solvent polarity or with time between absorption and emission. These data do not, however, preclude more subtle changes in the states involved. Such changes are in fact suggested by the smaller than expected variation of the transition moments with solvent.

The absorption and steady-state emission spectra of DCS vary systematically with solvent polarity. The variations observed

are reasonably correlated by the dielectric continuum measures of solvent polarity, and there is no evidence that hydrogen bonding or other specific solute−solvent interactions are of special significance to the spectroscopy. The absorption and emission spectra shift to the red with increasing solvent polarity, a feature which has been observed[12] and analyzed[10,11,20,76] several times already. What has not been previously analyzed is the systematic evolution of the vibronic structure of the electronic bands with solvent polarity. In the case of emission, the spectrum is highly structured in nonpolar solvents. This structured emission is lost even in solvents of modest polarity,[10] where only a single featureless band is observed. But, instead of broadening as might be anticipated because of inhomogeneous solvent interactions, the emission band narrows substantially with increasing polarity. Quite similar changes in absorption and emission band shapes to those observed here in DCS have recently been reported for several highly solvatochromic dyes by Painelli and co-workers,[61] who interpreted this behavior in terms of a two-state model.[59,60] Less pronounced changes were also noted for the solute coumarin 153 (C153)[68,77] and recently interpreted in an analogous manner by Matyushov and Newton.[63] In the present work, we used fits to an empirical single harmonic mode line shape to quantify the observed spectral changes and then attempted to model the solvent dependence in two ways.

The first model, the "independent-state" (IS) model, is the sort of model most often used when interpreting solvatochromic data. It assumes independent S_0 and S_1 states, each characterized by its dipole moment and polarizability, which interact with a continuum dielectric solvent. Using this model, we find that the observed solvatochromism of DCS can be reproduced to within experimental uncertainties only with sets of model parameters that are not entirely satisfactory. The problem resides in the large difference between the solvatochromic slopes C_{abs} and C_{em}, which can only be fit by making the ground-state dipole moment considerably smaller than the experimental value. (We note that the same type of modeling applied to the extensive data previously collected for the solute C153[68,72] does yield satisfactory fits.) Il'ichev et al.[10] previously reported this difficulty and interpreted it as implying distinct Franck−Condon and emitting S_1 states possessing substantially (8 D) different dipole moments. On the basis of the transition moment data obtained here, as well as the fact that electrochromic absorption[40] and emission[41] measurements in dioxane report the same value for the S_1 dipole moment (20 D), such a large change in μ_1 now seems unlikely. A more plausible explanation is that attempting to model the frequency data without properly accounting for changes to the vibronic structure with solvent is responsible for the less than ideal fit.

We therefore also examined the solvatochromic shifts of DCS data in light of a "coupled-state" (CS) model close in concept to those of Painelli[59,60] and Matyushov[46,62,63] mentioned above. This model considers the S_0 and S_1 states to arise from the solvent-modulated mixing of two valence states. As employed here, this model does not resolve the difficulty with fitting the solvent dependence of the frequencies. But it does provide a satisfying initial description of the large changes in the vibronic line shapes with solvent. It also predicts a modest variation of the emission transition moments with solvent. This trend does not appear to be present in the experimental data, presumably because of the involvement of more than two electronic states in the real system. Extension of the basic CS model to include perturbations by additional excited states, together with consideration of the distribution of solvation and vibrational states which were neglected here, could provide a more complete description of the experimental data and potentially explain the apparent inconsistency in the frequency shifts noted above. The latter problem might also be related to the simple point-dipole/spherical cavity representation of the solute employed in both models. Further investigation of these possibilities is warranted.

Finally, we have measured time-resolved emission spectra of DCS in a number of solvents with subpicosecond resolution. Our results corroborate and generalize those of Kovalenko et al.[28] who concluded on the basis of ~100 fs resolution absorption and emission measurements that spectral dynamics in acetonitrile reflect only time-dependent solvation. In contrast to other reports,[29,31] but in keeping with the results of Il'ichev et al.,[10,13] we do not find evidence for spectral changes that would signal the presence of more than one excited state. We observe only the continuous evolution of the spectra with time that is characteristic of solvent relaxation. The close correspondence between the normalized spectral response functions of DCS and C153 in 11 solvents clearly demonstrates that the spectral dynamics being observed in DCS also primarily reflect solvent relaxation.

Taken together, all of these results indicate that the spectroscopy of DCS does not involve multiple emitting states or other complex dynamics. The S_1 state appears to be a single electronic state whose character varies slightly with solvent polarity, largely as would be expected from a simple coupled-state description. This simplicity, the similarity of its spectral response to that of the well studied solvation probe C153, together with its favorable absorption and emission characteristics and larger Stokes shift (3000 vs 2000 cm^{-1} in highly polar solvents) suggest that DCS be considered a useful time-dependent solvation probe.

Acknowledgment. The authors thank Bernie O'Hare for measuring the NMR spectra of DCS and Dmitry Matyushov for correcting an error in our original formulation of the IS model described here. This work was supported by the Office of Basic Energy Sciences of the U.S. Department of Energy.

Appendix

"Independent-State" (IS) Model. We assume the solute to be a spherical cavity of radius a containing a centered point dipole of moment $\vec{\mu}_i$ and an isotropic polarizability α. The dipole moment depends on the solute electronic state ($i = 0$ or 1), but the cavity radius and polarizability are assumed to be the same in both states. The solvent is treated as a dielectric continuum characterized by its static dielectric constant ϵ and its refractive index n. Following Hynes,[78,79] we express the nonequilibrium free energy of each state as a function of the nuclear polarization of the surroundings "$\vec{\mu}_s$", by

$$F_i(\vec{\mu}_s) = U_i^0 - (1/2)(B_{el} + B_{el})\mu_i^2 + (1/2)B_{nuc}\{\vec{\mu}_i - \vec{\mu}_s\}^2 \quad \text{(A1)}$$

where U_i^0 is the gas-phase energy of state i and $B_{el}^{(i)}$ and $B_{nuc}^{(i)}$ are the electronic and nuclear polarization response functions of the solvent. The latter functions are represented by the dielectric continuum expressions[42]

$$B_{el} = \frac{f_{el}}{1 - \alpha f_{el}} \quad f_{el} = \frac{2}{a^3}\left(\frac{n^2 - 1}{2n^2 + 1}\right) \quad \text{(A2)}$$

$$B_{nuc} = \frac{f_{tot}}{1 - \alpha f_{tot}} - B_{el} \quad f_{tot} = \frac{2}{a^3}\left(\frac{\epsilon - 1}{2\epsilon + 1}\right) \quad \text{(A3)}$$

The solvent nuclear polarization is represented here by $\vec{\mu}_s$, the value of the solute dipole with which a given solvent nuclear polarization would be in equilibrium. Absorption and emission frequencies are assumed to be given by the differences between the minimum (equilibrium) free energy of the originating state of the transition "orig" where $\vec{\mu}_s = \vec{\mu}_{orig}$ and the free energy of the nonequilibrium final state has this same (Franck−Condon) value of solvent nuclear polarization. Thus

$$h\nu_{abs} = F_1^{FC} - F_0^{eq} = F_1(\vec{\mu}_0) - F_0(\vec{\mu}_0) + \lambda_{vib} \quad \text{(A4)}$$

$$h\nu_{em} = F_1^{eq} - F_0^{FC} = F_1(\vec{\mu}_1) - F_0(\vec{\mu}_1) - \lambda_{vib} \quad \text{(A5)}$$

The terms λ_{vib} are included to account for any vibrational reorganization energy associated with low-frequency vibrations of the solute not included in the vibronic fitting. These terms are added here rather than by including terms quadratic in some vibrational coordinate to eq A1 (as will be done later in model 2) to keep the notation as simple as possible.

Equations A1−A5 define the IS model. These equations are used directly for the "complete" analysis described in the text. For a fixed value of the solute polarizability, these expressions can be recast into the forms typically used for fitting solvatochromic data. Defining the reaction field factors

$$d_0(x) \equiv \frac{x-1}{2x+1} \quad \text{(A6)}$$

and

$$d_c(x) \equiv \frac{d_0(x)}{1 - 2cd_0(x)} \quad \text{(A7)}$$

the solvent response functions can be written

$$(1/2)B_{el} = \frac{1}{a^3} d_c(n^2) \quad \text{and} \quad (1/2)B_{tot} = \frac{1}{a^3} d_c(\epsilon) \quad \text{(A8)}$$

with $c = \alpha/a^3$, a dimensionless polarizability parameter. The absorption and emission frequencies then become

$$h\nu_{abs} = h\nu_{abs}^0 + A_{abs} d_c(n^2) + C_{abs}\{d_c(\epsilon) - d_c(n^2)\} \quad \text{(A9)}$$

$$h\nu_{em} = h\nu_{em}^0 + A_{em} d_c(n^2) + C_{em}\{d_c(\epsilon) - d_c(n^2)\} \quad \text{(A10)}$$

where

$$A_{abs} = -(\mu_1^2 - \mu_0^2)a^{-3} \quad C_{abs} = -2\vec{\mu}_0 \cdot (\vec{\mu}_1 - \vec{\mu}_0)a^{-3} \quad \text{(A11)}$$

$$A_{em} = -(\mu_1^2 - \mu_0^2)a^{-3} \quad C_{em} = -2\vec{\mu}_1 \cdot (\vec{\mu}_1 - \vec{\mu}_0)a^{-3} \quad \text{(A12)}$$

and

$$h\nu_{abs}^0 = U_1^0 - U_0^0 + \lambda_{vib} = \Delta F^0 + \lambda_{vib} \quad \text{(A13)}$$

$$h\nu_{em}^0 = U_1^0 - U_0^0 - \lambda_{vib} = \Delta F^0 - \lambda_{vib} \quad \text{(A14)}$$

"Coupled-State" (CS) Model. The "coupled-state" (CS) model assumes that, rather than being independent, the S_0 and S_1 states result from the mixing of two valence bond states of differing charge-transfer character. Many authors have examined models of this sort in the context of the spectroscopy of bimolecular electron donor−acceptor complexes[53,55] and transition metal complexes,[54,56] the electrooptical properties of "push−pull" molecules,[5,57−61] and in more general electron-transfer contexts.[46,62,63] Most work has focused on how polar solvation modifies the mixing of the states and thereby the ground-state properties and some spectroscopic observables. Recently, Painelli and co-workers[59,60] and Matyushov and Newton[63] have explored how electron-vibration coupling in the two-state model leads to a solvent-dependent vibronic structure. Our perspective shares much in common with these latter two approaches, as well as with the work of Hynes and co-workers.[58] Nevertheless, because our implementation differs in detail from that of all of these prior studies, we outline it below.

In the CS model, the S_0 and S_1 states are described in terms of a basis consisting of "neutral" (N) and "charge-transfer" (CT) valence bond states

$$|S_0\rangle = \chi^{1/2}|N\rangle + (1-\chi)^{1/2}|CT\rangle$$

$$|S_1\rangle = (1-\chi)^{1/2}|N\rangle - \chi^{1/2}|CT\rangle \quad \text{(A15)}$$

which mix according to the effective Hamiltonian

$$H_{el}(\vec{\mu}_s, Q) = \begin{pmatrix} F_N(\vec{\mu}_s, Q) & V_{el} \\ V_{el} & F_{CT}(\vec{\mu}_s, Q) \end{pmatrix} \quad \text{(A16)}$$

where the coupling matrix element V_{el} is assumed to be a constant. The free energies of the basis states are expressed as quadratic functions of a solvent polarization coordinate $\vec{\mu}_s$ and a vibrational coordinate Q in the manner

$$F_N(\vec{\mu}_s, Q) = -(1/2)B_{tot}\mu_N^2 + (1/2)B_{nuc}(\vec{\mu}_s - \vec{\mu}_N)^2 + (1/2)\hbar\omega(Q - Q_N)^2 \quad \text{(A17)}$$

$$F_{CT}(\vec{\mu}_s, Q) = \Delta E - (1/2)B_{tot}\mu_{CT}^2 + (1/2)B_{nuc}(\vec{\mu}_s - \vec{\mu}_{CT})^2 + (1/2)\hbar\omega(Q - Q_{CT})^2 \quad \text{(A18)}$$

where ΔE is the energy gap between the minima of the CT and N states in the absence of solvent, $\vec{\mu}_N$, and $\vec{\mu}_{CT}$ are the dipole moments, and Q_N and Q_{CT} the equilibrium vibrational coordinates of these basis states. A single vibrational mode of frequency ω is used to represent the net effect of all vibrations that are displaced between the N and CT states. For the solvent response functions, we use nonpolarizable versions of the dielectric continuum expressions eqs A2 and A3, which can be written

$$(1/2)B_{el} = \frac{1}{a^3} d_0(n^2) \quad \text{and} \quad (1/2)B_{tot} = \frac{1}{a^3} d_0(\epsilon) \quad \text{(A19)}$$

The free energies of the S_0 and S_1 states obtained by solving eq A16 are

$$F_0(\vec{\mu}_s, Q) = (1/2)\{(F_N + F_{CT}) - \sqrt{(F_{CT} - F_N)^2 + 4V_{el}^2}\}$$

$$F_1(\vec{\mu}_s, Q) = (1/2)\{(F_N + F_{CT}) + \sqrt{(F_{CT} - F_N)^2 + 4V_{el}^2}\} \quad \text{(A20)}$$

and the mixing coefficient χ is given by

$$\chi(\vec{\mu}_s, Q) = \left(\frac{V_{el}^2}{V_{el}^2 + (F_N - F_0)^2}\right) = \frac{1}{2} + \frac{1}{2}\left(\frac{(F_{CT} - F_N)^2}{(F_{CT} - F_N)^2 + 4V_{el}^2}\right)^{1/2} \quad \text{(A21)}$$

For the sake of comparison, we note that this mixing coefficient is related to the ionicity parameter ρ used by Painelli and coworkers[59,60] and the fractional zwitterionic character f used by Thompson et al.[58] by $\chi = 1 - \rho = 1 - f$.

Equations A15−A20 describe two-dimensional surfaces in $\vec{\mu}_s$ and Q. For purposes of modeling the spectral frequencies and their solvent variation, we only consider the minima in these surfaces and their Franck−Condon projections.

$$h\nu_{abs} = F_1^{FC} - F_0^{eq} = F_1(\vec{\mu}_0,Q_0) - F_0(\vec{\mu}_0,Q_0) \quad \text{(A22)}$$

$$h\nu_{em} = F_1^{eq} - F_0^{FC} = F_1(\vec{\mu}_1,Q_1) - F_0(\vec{\mu}_1,Q_1) \quad \text{(A23)}$$

where $(\vec{\mu}_0,Q_0)$ and $(\vec{\mu}_1,Q_1)$ denote the locations of the minima, which are given by

$$\vec{\mu}_0 = \chi\vec{\mu}_N + (1-\chi)\vec{\mu}_{CT} \quad Q_0 = \chi Q_N + (1-\chi)Q_{CT} \quad \text{(A24)}$$

$$\vec{\mu}_1 = \chi\vec{\mu}_{CT} + (1-\chi)\vec{\mu}_N \quad Q_1 = \chi Q_{CT} + (1-\chi)Q_N \quad \text{(A25)}$$

Equations A24 and A25 are obtained, for example, by writing $F_0 = \chi F_N + 2(\chi(1-\chi))^{1/2}V_{el} + (1-\chi)F_{CT}$ and differentiating with respect to $\vec{\mu}_s$ to determine $\vec{\mu}_0$, and so forth.

It is useful to rewrite eqs A17 and A18 in the more compact forms

$$F_N = -(1/2)B_{tot}\mu_N^2 + \lambda_{solv}x_{solv}^2 + \Lambda_{vib}x_{vib}^2 \quad \text{(A26)}$$

$$F_{CT} = \Delta E - (1/2)B_{tot}\mu_{CT}^2 + \lambda_{solv}(x_{solv}-1)^2 + \Lambda_{vib}(x_{vib}-1)^2 \quad \text{(A27)}$$

by defining the dimensionless variables

$$\vec{x}_{solv} = (\vec{\mu}_s - \vec{\mu}_N)/|\vec{\mu}_{CT} - \vec{\mu}_N| \qquad x_{vib} = (Q - Q_N)/(Q_{CT} - Q_N) \quad \text{(A28)}$$

and reorganization energies

$$\lambda_{solv} = (1/2)B_{nuc}(\vec{\mu}_{CT} - \vec{\mu}_{LE})^2 \qquad \Lambda_{vib} = (1/2)\hbar\omega(Q_{CT} - Q_{LE})^2 \quad \text{(A29)}$$

Note that we use the symbol Λ_{vib} here rather than λ_{vib} to distinguish this quantity from λ_{vib} used in the IS model. Whereas, in the former model, λ_{vib} only contained the "classical" vibrational reorganization energy not accounted for in the vibronic fits, Λ_{vib} here includes contributions from all modes displaced in $|CT\rangle$ relative to $|N\rangle$. The frequencies of interest can then be written in terms of the mixing coefficient χ as

$$h\nu_{abs} = F_1(x = 1-\chi_0) - F_0(x = 1-\chi_0) \quad \text{(A30)}$$

$$h\nu_{em} = F_1(x = \chi_1) - F_0(x = \chi_1) \quad \text{(A31)}$$

where x is used to denote all components of $\vec{x}_{solv}$ and x_{vib}, which are all equal at the minima. It is important to note that the free energies F_N and F_{CT} (eqs A26 and A27) needed to calculate ν_{abs} and ν_{em} depend on χ, which in turn depends on F_N and F_{CT} via eq A21. Thus, calculations must be carried out in an iterative manner to achieve self-consistency in χ. This self-consistency requirement also means that the value of χ will not be the same in the equilibrium ground and excited states, and this fact is denoted by the subscripts on χ in eqs A30 and A31. Once the appropriate value of χ is determined, the frequencies can be expressed quite simply by noting that the vertical gap F_1-F_0 for any values of $\vec{x}_{solv}$ and x_{vib} is equal to $V_{el}/(\chi(1-\chi))^{1/2}$. Thus

$$h\nu_{abs} = \frac{V_{el}}{\sqrt{\chi_0(1-\chi_0)}} \quad h\nu_{em} = \frac{V_{el}}{\sqrt{\chi_1(1-\chi_1)}} \quad \text{(A32)}$$

A number of properties of the S_0 and S_1 states other than the transition frequencies are of interest for comparisons to experiment and the IS model. When the standard assumption that $\langle N|\vec{\mu}|CT\rangle = 0$ is made, the dipole moments of the equilibrium S_0 and S_1 states and the transition moments connecting them can be written

$$\vec{\mu}_0 = \chi_0\vec{\mu}_N + (1-\chi_0)\vec{\mu}_{CT} \quad \vec{\mu}_1 = \chi_1\vec{\mu}_{CT} + (1-\chi_1)\vec{\mu}_N \quad \text{(A33)}$$

$$|M_{abs}| = \{\chi_0(1-\chi_0)\}^{1/2}|\vec{\mu}_{CT} - \vec{\mu}_{LE}| \qquad |M_{em}| = \{\chi_1(1-\chi_1)\}^{1/2}|\vec{\mu}_{CT} - \vec{\mu}_{LE}| \quad \text{(A34)}$$

Combining eqs A34 with A32 provides the important prediction that the transition moments should be inversely proportional to the transition frequencies

$$|M_x| = \frac{|\vec{\mu}_{CT} - \vec{\mu}_{LE}|V_{el}}{h\nu_x} \quad (x = \text{abs, em}) \quad \text{(A35)}$$

The polarizabilities of the equilibrium S_0 and S_1 states are[58,80]

$$\alpha_0 = 2\{\chi_0(1-\chi_0)\}^{3/2}\frac{|\vec{\mu}_{CT} - \vec{\mu}_{LE}|}{V_{el}} \qquad \alpha_1 = -2\{\chi_1(1-\chi_1)\}^{3/2}\frac{|\vec{\mu}_{CT} - \vec{\mu}_{LE}|}{V_{el}} \quad \text{(A36)}$$

Note that within this description the polarizability of S_1 is negative, which is an unrealistic feature of two-state models.

Finally, the effect of electronic state mixing on the vibronic structure of the absorption and emission can be described by the Huang−Rhys factors, $S = (1/2)(Q_1 - Q_0)$, which are given by

$$S'_{abs} = (1/2)(1-\chi_0)^2(Q_{CT} - Q_N)^2 = (1-2\chi_0)^2\frac{\Lambda_{vib}}{\hbar\omega} \quad \text{(A37)}$$

$$S'_{em} = (1/2)(1-\chi_1)^2(Q_{CT} - Q_N)^2 = (1-2\chi_1)^2\frac{\Lambda_{vib}}{\hbar\omega} \quad \text{(A38)}$$

The primes here are used to indicate that these values should not be directly compared to the Huang−Rhys factors S_x obtained from the experimental spectra. The S'_x values here are calculated from the total vibrational reorganization energies Λ_{vib}, which includes contributions from both high- and low-frequency modes. S_{abs} and S_{em} from experiment, on the other hand, are used to characterize the shape of the spectrum, which is due to only the single, effective high-frequency mode that gives rise to the vibronic progression apparent in nonpolar solvents. We approximate the experimental quantities in the CS model by assuming that

$$S_i = (1-2\chi_i)^2(\Lambda_{vib} - \lambda_{vib})/\hbar\omega \quad \text{(A39)}$$

where λ_{vib} is the low-frequency portion of the vibrational reorganization energy, estimated from the experimental analysis of the "0−0" frequency data.

Supporting Information Available: Emission spectra of DCS in *n*-hexane and diisopropylether mixtures and character-

istics of the emission spectra of these mixtures obtained from fits to eq 3. This material is available free of charge via the Internet at http://pubs.acs.org.

References and Notes

(1) Görner, H.; Kuhn, H. J. *Adv. Photochem.* **1995**, *19*, 1−117.

(2) Papper, V.; Pines, D.; Likhtenshtein, G.; Pines, E. *J. Photochem. Photobiol., A* **1997**, *111*, 87−96.

(3) Liptay, W. In *Excited States*; Lim, E. C., Ed.; Academic Press: New York, 1974; Vol. 1, pp 129−229.

(4) Barzoukas, M.; Fort, A.; Klein, G.; Serbutoviez, C.; Oswald, L.; Nicoud, J. F. *Chem. Phys.* **1992**, *164*, 395−406.

(5) Barzoukas, M.; Runser, C.; Fort, A.; Blanchard-Desce, M. *Chem. Phys. Lett.* **1996**, *257*, 531−537.

(6) Lippert, E. *Z. Elektrochem. Angew. Phys. Chem.* **1957**, *61*, 962−975.

(7) Czekalla, J. *Z. Elektrochem. Angew. Phys. Chem.* **1960**, *64*, 1221−1228.

(8) Kawski, A.; Kubicki, A. *Acta Phys. Pol., A* **1991**, *79*, 457−470.

(9) Lapouyade, R.; Czeschka, K.; Majenz, W.; Rettig, W.; Gilabert, E.; Rulliere, C. *J. Phys. Chem.* **1992**, *96*, 9643−9650.

(10) Il'ichev, Y. V.; Kühnle, W.; Zachariasse, K. A. *Chem. Phys.* **1996**, *211*, 441−453.

(11) Lewis, F.; Weigel, W. *J. Phys. Chem. A* **2000**, *104*, 8146−8153.

(12) Gruen, H.; Görner, H. *Z. Naturforsch., A: Phys. Sci.* **1983**, *38*, 928−936.

(13) Il'ichev, Y. V.; Zachariasse, K. A. *Ber. Bunsen-Ges. Phys. Chem.* **1997**, *101*, 625−635.

(14) Lapouyade, R.; Kuhn, A.; Letard, J.-F.; Rettig, W. *Chem. Phys. Lett.* **1993**, *208*, 48−58.

(15) Dekhtyar, M.; Rettig, W. *Phys. Chem. Chem. Phys.* **2001**, *3*, 1602−1610.

(16) Amatatsu, Y. *Theor. Chem. Acc.* **2000**, *103*, 445−450.

(17) Amatatsu, Y. *Chem. Phys.* **2001**, *274*, 87−98.

(18) Amatatsu, Y. *Chem. Phys. Lett.* **2003**, *369*, 673−679.

(19) Schroeder, J.; Steinel, T.; Troe, J. *J. Phys. Chem. A* **2002**, *106*, 5510−5516.

(20) Rijkenberg, R. A.; Bebelaar, D.; Buma, W. J.; Hofstraat, J. W. *J. Phys. Chem. A* **2002**, *106*, 2446−2456.

(21) Daum, R.; Hansson, T.; Noerenberg, R.; Schwarzer, D.; Schroeder, J. *Chem. Phys. Lett.* **1995**, *246*, 607−614.

(22) Safarzadeh-Amiri, A. *Chem. Phys. Lett.* **1986**, *125*, 272−278.

(23) Gilabert, E.; Lapouyade, R.; Rulliere, C. *Chem. Phys. Lett.* **1988**, *145*, 262−268.

(24) Gilabert, E.; Lapouyade, R.; Rulliere, C. *Chem. Phys. Lett.* **1991**, *185*, 82−87.

(25) Rettig, W.; Gilabert, E.; Rulliere, C. *Chem. Phys. Lett.* **1994**, *229*, 127−133.

(26) Abraham, E.; Oberle, J.; Jonusauskas, G.; Lapouyade, R.; Minoshima, K.; Rulliere, C. *Chem. Phys.* **1997**, *219*, 73−89.

(27) Abraham, E.; Oberle, J.; Jonusauskas, G.; Lapouyade, R.; Rulliere, C. *Chem. Phys.* **1997**, *214*, 409−423.

(28) Kovalenko, S. A.; Schanz, R.; Senyushkina, T. A.; Ernsting, N. P. *Phys. Chem. Chem. Phys.* **2002**, *4*, 703−707.

(29) Pines, D.; Pines, E.; Rettig, W. *J. Phys. Chem. A* **2003**, *107*, 236−242.

(30) Rettig, W.; Majenz, W. *Chem. Phys. Lett.* **1989**, *154*, 335−341.

(31) Eilers-Koenig, N.; Küehne, T.; Schwarzer, D.; Voehringer, P.; Schroeder, J. *Chem. Phys. Lett.* **1996**, *253*, 69−76.

(32) Velapoldi, R.; Mielenz, K. *A Fluorescence Standard Reference Material: Quinine Sulfate Dihydrate*; National Bureau of Standards: Washington, DC, 1980; Vol. Special Publications, pp 260−264.

(33) Dahl, K.; Biswas, R.; Ito, N.; Maroncelli, M. *J. Phys. Chem. B* **2005**, *109*, 1563−1585.

(34) Arzhantsev, S.; Maroncelli, M. *Appl. Spectrosc.* **2005**, *59*, 206−220.

(35) Frisch, M. J.; Trucks, G. W.; Schlegel, H. B.; Scuseria, G. E.; Robb, M. A.; Cheeseman, J. R.; Montgomery, J. A., Jr.; Vreven, T.; Kudin, K. N.; Burant, J. C.; Millam, J. M.; Iyengar, S. S.; Tomasi, J.; Barone, V.; Mennucci, B.; Cossi, M.; Scalmani, G.; Rega, N.; Petersson, G. A.; Nakatsuji, H.; Hada, M.; Ehara, M.; Toyota, K.; Fukuda, R.; Hasegawa, J.; Ishida, M.; Nakajima, T.; Honda, Y.; Kitao, O.; Nakai, H.; Klene, M.; Li, X.; Knox, J. E.; Hratchian, H. P.; Cross, J. B.; Adamo, C.; Jaramillo, J.; Gomperts, R.; Stratmann, R. E.; Yazyev, O.; Austin, A. J.; Cammi, R.; Pomelli, C.; Ochterski, J. W.; Ayala, P. Y.; Morokuma, K.; Voth, G. A.; Salvador, P.; Dannenberg, J. J.; Zakrzewski, V. G.; Dapprich, S.; Daniels, A. D.; Strain, M. C.; Farkas, O.; Malick, D. K.; Rabuck, A. D.; Raghavachari, K.; Foresman, J. B.; Ortiz, J. V.; Cui, Q.; Baboul, A. G.; Clifford, S.; Cioslowski, J.; Stefanov, B. B.; Liu, G.; Liashenko, A.; Piskorz, P.; Komaromi, I.; Martin, R. L.; Fox, D. J.; Keith, T.; Al-Laham, M. A.; Peng, C. Y.; Nanayakkara, A.; Challacombe, M.; Gill, P. M. W.; Johnson, B.; Chen, W.; Wong, M. W.; Gonzalez, C.; Pople, J. A. *GAUSSIAN03*, revision C.01; Gaussian, Inc.: Wallingford, CT, 2004.

(36) *AMPAC 8*, version 8.15; Semichem, Inc.: Shawnee, KS, 1992−2004. Details of the CI procedures used can be found in http://www.semichem.com/ampacmanual/.

(37) Kwasniewski, S. P.; Claes, L.; Francois, J. P.; Deleuze, M. S. *J. Chem. Phys.* **2003**, *118*, 7823−7836.

(38) Rotational coherence measurements of jet-cooled molecules[21] were originally interpreted as suggesting that DCS is nonplanar in both S_0 and S_1. But these data are also consistent with molecules executing large-amplitude torsional motions about a planar geometry.

(39) Champagne, B. B.; Pfanstiel, J. F.; Plusquellic, D. F.; Pratt, D. W.; van Herpen, W. M.; Meerts, W. L. *J. Phys. Chem.* **1990**, *94*, 6−8.

(40) Czekalla, J.; Wick, G. *Z. Elektrochem. Angew. Phys. Chem.* **1961**, *65*, 727−734.

(41) Czekalla, J.; Liptay, W.; Meyer, K. O. *Ber. Bunsen-Ges. Phys. Chem.* **1963**, *67*, 465−470.

(42) Böttcher, C. J. F.; van Belle, O. C.; Bordewijk, P.; Rip, A. *Theory of Electric Polarization: Dielectrics in Static Fields*; Elsevier: Amsterdam, The Netherlands, 1973; Vol. I.

(43) Marcus, R. A. *J. Phys. Chem.* **1989**, *93*, 3078−3086.

(44) Birks, J. B. *Photophysics of Aromatic Molecules*; Wiley: London, 1970.

(45) Lewis, J. E.; Maroncelli, M. *Chem. Phys. Lett.* **1998**, *282*, 197−203.

(46) Matyushov, D.; Voth, G. *J. Phys. Chem. A* **2000**, *104*, 6485−6494.

(47) Gould, I. R.; Young, R. H.; Mueller, L. J.; Albrecht, A. C.; Farid, S. *J. Am. Chem. Soc.* **1994**, *116*, 8188−8199.

(48) Hirayama, S.; Phillips, D. *J. Photochem.* **1980**, *12*, 139−145.

(49) This value of $c = \alpha/a^3$ was estimated from a series of AM1 calculations of the ground state of DCS using the COSMO self-consistent reaction field method[84] at a series of solvent dielectric constants (with a solvent radius of 1.5 Å). These data were fit to the relation[42] $\mu(\epsilon = 1)/\mu(\epsilon) = 1 - 2cd_0(\epsilon)$, where $d_0(x)$ is defined by eq 4.

(50) This parameter is defined by $\chi_\nu^2 = (1/\nu)\,\Sigma_i\{y_i(\text{obs}) - y_i(\text{fit})\}^2/\sigma_i^2$ where y_i values represent the quantities being fit, σ_i, their estimated uncertainties, and ν the number of degrees of freedom in the fit (the number of independent data points minus the number of model parameters varied).

(51) Bevington, P. R. *Data Reduction and Error Analysis for the Physical Sciences*; McGraw-Hill: New York, 1969.

(52) Through the use of van der Waals increments,[85] the van der Waals volume of DCS is estimated to be 244 Å^3. A sphere of this volume has a radius of 3.9 Å. This "bare" solute radius would yield estimates of solvation energies that are too large. A better first guess is this radius increased by an average solvent molecule radius of ∼1.5 Å which would give a value of $a = 5.4$ Å. But, the solute is not spherical and it is better to employ a method that takes the actual shape of the solute into account. We have such information available from the COSMO/AM1 calculations used to estimate the value of α/a^3 (see note 49). Through the use of the value $\alpha/a^3 = 0.235$ and the empirical relation between molecular volumes and polarizability, $\alpha \cong 0.0268V_{\text{vdW}}^{1.35}$, a value of $a = 5.75$ Å is estimated.

(53) Mulliken, R. S. *J. Am. Chem. Soc.* **1952**, *74*, 811−824.

(54) Hush, N. S. *Prog. Inorg. Chem.* **1968**, *8*, 391.

(55) Gould, I. R.; Noukakis, D.; Gomez-Jahn, L.; Young, R. H.; Goodman, J. L.; Farid, S. *Chem. Phys.* **1993**, *176*, 439−456.

(56) Creutz, C.; Newton, M. D.; Sutin, N. *J. Photochem. Photobiol., A* **1994**, *82*, 47−59.

(57) Chen, G.; Lu, D.; Goddard, W. A., III. *J. Chem. Phys.* **1994**, *101*, 5860−5864.

(58) Thompson, W. H.; Blanchard-Desce, M.; Hynes, J. T. *J. Phys. Chem. A* **1998**, *102*, 7712−7722.

(59) Painelli, A.; Terenziani, F. *Chem. Phys. Lett.* **1999**, *312*, 211−220.

(60) Painelli, A.; Terenziani, F. *J. Phys. Chem. A* **2000**, *104*, 11041−11048.

(61) Boldrini, B.; Cavalli, E.; Painelli, A.; Terenziani, F. *J. Phys. Chem. A* **2002**, *106*, 6286−6294.

(62) Matyushov, D.; Voth, G. *J. Phys. Chem. A* **2000**, *104*, 6470−6484.

(63) Matyushov, D.; Newton, M. *J. Phys. Chem. A* **2001**, *105*, 8516−8532.

(64) Cave, R.; Newton, M. *Chem. Phys. Lett.* **1996**, *249*, 15−19.

(65) Bixon, M.; Jortner, J.; Verhoeven, J. *J. Am. Chem. Soc.* **1994**, *116*, 7349−7355.

(66) Kohler, G.; Rechthaler, K.; Grabner, G.; Luboradzki, R.; Suwinska, K.; Rotkiewicz, K. *J. Phys. Chem. A* **1997**, *101*, 8518−8525.

(67) Gustavsson, T.; Cassara, L.; Gulbinas, V.; Gurzadyan, G.; Mialocq, J.-C.; Pommeret, S.; Sorgius, M.; Muelen, P. v. d. *J. Phys. Chem. A* **1998**, *102*, 4229−4245.

(68) Horng, M. L.; Gardecki, J. A.; Papazyan, A.; Maroncelli, M. *J. Phys. Chem.* **1995**, *99*, 17311−17337.

(69) Cave, R. J.; Castner, E. W., Jr. *J. Phys. Chem. A* **2002**, *106*, 12117−12123.

(70) Muhlpfordt, A.; Schanz, R.; Ernsting, N.; Farztdinov, V.; Grimme, S. *Phys. Chem. Chem. Phys.* **1999**, *1*, 3209−3218.
(71) Maroncelli, M. *J. Chem. Phys.* **1997**, *106*, 1545−1555.
(72) Reynolds, L.; Gardecki, J. A.; Frankland, S. J. V.; Horng, M. L.; Maroncelli, M. *J. Phys. Chem.* **1996**, *100*, 10337−10354.
(73) Ingrosso, F.; Ladanyi, B. M.; Mennucci, B.; Elola, M. D.; Tomasi, J. *J. Phys. Chem. B* **2005**, *109*, 3553−3564.
(74) Song, X.; Chandler, D. *J. Chem. Phys.* **1998**, *108*, 2594−2600.
(75) Kumar, P. V.; Maroncelli, M. *J. Chem. Phys.* **1995**, *103*, 3038−3060.
(76) Lippert, E. *Z. Naturforsch., A: Phys. Sci.* **1955**, *10*, 541−545.
(77) Maroncelli, M.; Fleming, G. R. *J. Chem. Phys.* **1987**, *86*, 6221−6239.
(78) van der Zwan, G.; Hynes, J. T. *J. Phys. Chem.* **1985**, *89*, 4181−4188.
(79) Hynes, J. T. In *Ultrafast Dynamics of Chemical Systems*; Simon, J. D., Ed.; Kluwer: Dordrecht, The Netherlands, 1994; pp 345−381.
(80) Painelli, A. *Chem. Phys. Lett.* **1998**, *285*, 352−358.
(81) Marcus, Y. *The Properties of Solvents*; Wiley: New York, 1998.
(82) Lakowicz, J. R.; Gryczynski, I.; Laczko, G.; Gloyna, D. *J. Fluoresc.* **1991**, *1*, 87−93.
(83) K. A. Zachariasse, unpublished data on UV−vis spectra of component spectra of DCS in CH_3Cl + isooctane separated using HPLC.
(84) Klampt, A. *J. Phys. Chem.* **1995**, *99*, 2224−2235.
(85) Bondi, A. *J. Phys. Chem.* **1964**, *68*, 441−451.